Elastic Deformation due to Polygonal Dislocations in a Transversely Isotropic Half-Space

Article *in* Bulletin of the Seismological Society of America · December 2014

DOI: 10.1785/0120140161

CITATIONS
9

READS
77

4 authors:

Evgheni Pan
Vilnius Gediminas Technical University
264 PUBLICATIONS **6,855** CITATIONS
SEE PROFILE

Jianghong Yuan
Tsinghua University
8 PUBLICATIONS **29** CITATIONS
SEE PROFILE

W. Q. Chen
Zhejiang University
500 PUBLICATIONS **8,622** CITATIONS
SEE PROFILE

William Ashley Griffith
The Ohio State University
73 PUBLICATIONS **557** CITATIONS
SEE PROFILE

Bulletin of the Seismological Society of America, Vol. 104, No. 6, pp. 2698–2716, December 2014, doi: 10.1785/0120140161

Ⓔ

Elastic Deformation due to Polygonal Dislocations in a Transversely Isotropic Half-Space

by E. Pan, J. H. Yuan,* W. Q. Chen, and W. A. Griffith

Abstract Based upon the fundamental solution to a single straight dislocation segment, a complete set of exact closed-form solutions is presented in a unified manner for elastic displacements and strains due to general polygonal dislocations in a transversely isotropic half-space. These solutions are systematically composed of two parts: one representing the solution in an infinite transversely isotropic medium and the other accounting for the influence of the free surface of the half-space. Numerical examples are provided to illustrate the effect of material anisotropy on the elastic displacement and strain fields associated with dislocations. It is shown that if the rock mass is strongly anisotropic, surface displacements calculated using an isotropic model may result in errors greater than 20%, and some of the strain components near the fault tip may vary by over 200% compared with the transversely isotropic model. Even for rocks with weak anisotropy, the strains based on the isotropic model can also result in significant errors. Our analytical solutions along with the corresponding MATLAB source codes can be used to predict the static displacement and strain fields due to earthquakes, particularly when the rock mass in the half-space is best approximated as transversely isotropic, as is the case for most sedimentary basins.

Online Material: MATLAB scripts to calculate rectangular and triangular dislocations in a transversely isotropic half-space.

Introduction

Analytical solutions for dislocations of simple geometries provide a useful means for inferring the behavior of faults and intrusions at depth using remotely sensed data on the Earth's surface (Segall, 2007, and references therein). Early approaches were limited to two dimensions, utilizing analytical solutions for screw dislocations to study strike-slip faults (e.g., Thatcher, 1975), edge dislocations as models of dip-slip faults (e.g., Freund and Barnett, 1976), as well as pressurized crack models of intrusive processes (e.g., Delaney and Pollard, 1981). Extending the approach to three dimensions, Okada's analytical solutions (Okada, 1985, 1992) for rectangular faults received substantial applications in geophysics due to their analytical nature. Applications of the rectangular fault model in the field of geodesy are also very diverse and vary from inferring dike propagation history (e.g., Yun *et al.*, 2006; Amelung *et al.*, 2007) to spatial and temporal reconstructions of earthquake slip (e.g., Johnsson *et al.*, 2002; Segall, 2007, and references therein) from surface displacements measured using Interferometric Synthetic Aperture Radar and Global Positioning System data. King *et al.* (1994) showed that static Coulomb stress changes calculated using rectangular dislocation models can be used as a triggering predictor, as positive Coulomb stress changes are typically associated with regions of large aftershock densities. Following an approach similar to King *et al.* (1994), Micklethwaite and Cox (2004) showed that static stress changes calculated using the rectangular dislocation model can be utilized to pinpoint potential locations of hydrothermal mineral deposits and related precious metals.

Although rectangular dislocations (or displacement discontinuities) are useful in fault deformation analysis, polygonal elements (such as triangular dislocations) allow a greater flexibility when the model surfaces (faults, joints, intrusions, and bedding discontinuities) are complex in three dimensions (Maerten *et al.*, 2014). Jeyakumaran *et al.* (1992) derived the triangular dislocation solution by superposing the solution for angular dislocations in an isotropic half-space (Yoffe, 1960, 1961; Comninou and Dunders, 1975). Thomas (1993) utilized the triangular dislocation solution in an isotropic linear elastic half-space to develop the code *Poly3D*. *Poly3D* has now been used by dozens of researchers on studies of complex geological discontinuities ranging from earthquake hazards (Griffith and Cooke, 2004; Maerten *et al.*,

*Also at the Center for Mechanics and Materials, Tsinghua University, Beijing 100084, China.

2005) to reservoir geomechanics (Maerten *et al.*, 2002; Chan and Zoback, 2007). A detailed and reliable algorithm for the calculation of triangular dislocation-induced displacement, strain, and stress fields was presented by Meade (2007), who also made the source code available for convenient implementation. Very recently, Maerten *et al.* (2014) presented a review of the development and applications of *Poly3D*, which later became known as *iBem3D*. Together, *Poly3D* and *iBem3D* found applications in over 130 published papers (Maerten *et al.*, 2014). Many of these studies focused on deformation induced by faults in sedimentary basins where the assumption of isotropy presents some limitations (e.g., Griffith and Cooke, 2004; Muller *et al.*, 2006).

Although the assumption of material isotropy is often appropriate in crystalline basement rocks, sedimentary rock masses are best described as transversely isotropic with the sedimentary bedding parallel to the plane of isotropy (Amadei, 1996; Wang and Liao, 1998; Gercek, 2007). Furthermore, a dislocation of polygonal shape is more convenient to approximate the shapes of real discontinuities, particularly when the discontinuities are represented by meshes of multiple connected polygonal elements. Therefore, it would be more desirable if the half-space can be transversely isotropic and the dislocation can be of a general polygonal shape, which motivates the present study. This article is organized as follows. In the Problem Description section, the problems to be solved will be defined, along with a brief introduction of the linear elastic material constants used to characterize the transversely isotropic solid. In the Point-Source Solutions in a Transversely Isotropic Half-Space section, we summarize the point-force and point-dislocation solutions in a transversely isotropic half-space. In the Finite-Dislocation Solutions in a Transversely Isotropic Half-Space section, we derive the finite-dislocation solution in a transversely isotropic half-space; and, in the Polygonal-Source Solutions in a Transversely Isotropic Half-Space section, based on the fundamental solution to a straight dislocation segment, the elastic displacements and strains due to polygonal strike-slip faults, dip-slip faults, and tensile fractures are obtained in exact closed forms. Finally, in the Numerical Examples section, we provide numerical examples to verify the correctness of the derived solutions and to illustrate the influence of material anisotropy on the elastic displacement and strain fields around simple rectangular and triangular dislocations. We summarize our work in the Conclusions section. Ⓔ Solutions provided here are also available in the electronic supplement to this article in the form of four individual MATLAB codes. Exact closed-form expressions for the displacement and distortion fields due to a straight segment of the dislocation loop are given in Appendix A. These expressions are written in terms of the functions directly used in the MATLAB programs. The function relations between those defined in this article and those in the MATLAB codes are listed in Appendix B.

Problem Description

Figure 1 shows a transversely isotropic half-space with an embedded dislocation of polygonal shape. A global

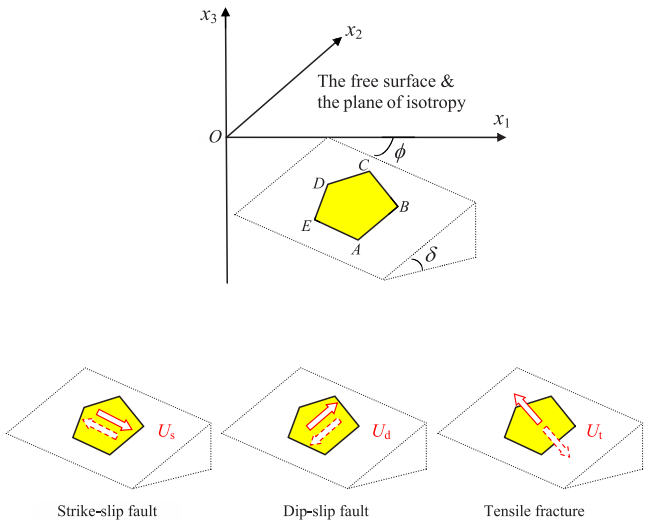

Figure 1. Geometry of a polygonal dislocation *ABCDE* with three types of discontinuities U_s, U_d, and U_t in a transversely isotropic half-space (with x_1–x_2 being the plane of isotropy and $x_3 = 0$ being the free surface). In this figure, $U_s > 0$, $U_d > 0$, $U_t > 0$, $\delta > 0$, and $\phi < 0$. The color version of this figure is available only in the electronic edition.

Cartesian coordinate system is drawn such that the x_1–x_2 plane is the free surface of the half-space, and $x_3 \leq 0$ is the problem domain. We assume the symmetry axis of the transversely isotropic material is parallel to the x_3 axis (i.e., the plane of isotropy of the transversely isotropic material is parallel to the x_1–x_2 plane). The strike-slip, dip-slip, and tensile components of the dislocation are denoted by U_s, U_d, and U_t, respectively, and each component represents the movement of the hanging-wall-side block relative to the foot-wall-side block. The strike direction of the fault relative to the x_1 axis is characterized by the rotation angle ϕ, and the dip angle of the fault is characterized by the inclined angle δ. The main goal of this article is to derive the expressions of the displacements and strains at any field point $\mathbf{x}(x_1, x_2, x_3)$ due to a general polygonal dislocation arbitrarily embedded in the transversely isotropic half-space.

In this article, summation over a repeated (or multiple-repeated) index is assumed unless this index occurs on both sides of an equation. Also, the range of values of Roman indexes (i, j, k, etc.) is 1, 2, 3, whereas the range of values for Greek letters (α, β, γ, etc.) is 1, 2, unless otherwise specified. For example, in the equation $D_{ij} = A_\alpha B_{i\alpha} C_{i\alpha}$, $i(= 1, 2, 3)$ is a free index without summation because it occurs on both sides of this equation, whereas α is a dummy index that should be summed from 1 to 2 because it occurs only on the right side of this equation and repeats itself three times. The single index $j(= 1, 2, 3)$ on the left side of the above equation is also a free index that indicates $D_{i1} = D_{i2} = D_{i3}$.

For a transversely isotropic material, if the plane of isotropy is parallel to the x_1–x_2 plane, then the elastic stiffness tensor c_{ijkl} can be expressed as

$$
\begin{aligned}
c_{ijkl} &= (c_{11}-2c_{66})\delta_{ij}\delta_{kl}+c_{66}(\delta_{ik}\delta_{jl}+\delta_{il}\delta_{jk})\\
&+(c_{11}+c_{33}-2c_{13}-4c_{44})\delta_{i3}\delta_{j3}\delta_{k3}\delta_{l3}\\
&+(c_{13}-c_{11}+2c_{66})(\delta_{i3}\delta_{j3}\delta_{kl}+\delta_{k3}\delta_{l3}\delta_{ij})\\
&+(c_{44}-c_{66})(\delta_{j3}\delta_{k3}\delta_{il}+\delta_{i3}\delta_{l3}\delta_{jk}+\delta_{j3}\delta_{l3}\delta_{ik}\\
&+\delta_{i3}\delta_{k3}\delta_{jl}) \qquad (1)
\end{aligned}
$$

(Pan and Chou, 1976), in which δ_{ij} is the Kronecker delta; c_{11}, c_{13}, c_{33}, c_{44}, and c_{66} are the five independent elastic stiffness constants.

Two basic sets of material constants (see Fabrikant, 2004), which will be used frequently in this article, are defined as

$$
\begin{aligned}
m_{1,2} &= -1+\frac{1}{2c_{44}(c_{13}+c_{44})}\\
&\times\left[(c_{11}c_{33}-c_{13}^2)\pm\sqrt{c_{11}c_{33}-c_{13}^2}\sqrt{c_{11}c_{33}-(c_{13}+2c_{44})^2}\right] \qquad (2)
\end{aligned}
$$

and

$$
\begin{aligned}
\gamma_\alpha &\equiv \frac{1}{s_\alpha}=\sqrt{\frac{c_{44}+m_\alpha(c_{13}+c_{44})}{c_{11}}}=\sqrt{\frac{m_\alpha c_{33}}{m_\alpha c_{44}+(c_{13}+c_{44})}},\\
\gamma_3 &\equiv \frac{1}{s_3}=\sqrt{\frac{c_{44}}{c_{66}}}, \qquad (3)
\end{aligned}
$$

with

$$
\begin{aligned}
m_1 m_2 &= 1,\\
m_1-m_2 &= \Theta(\gamma_1-\gamma_2), \quad \text{and}\\
\Theta &= c_{11}(\gamma_1+\gamma_2)/(c_{13}+c_{44}). \qquad (4)
\end{aligned}
$$

In equation (2), m_1 and m_2 correspond to the result on the right side of the equation with plus and minus signs, respectively. We point out that these expressions and the solutions derived below are based on the assumption that the material is a non-degenerate transversely isotropic material. In other words, for this material, $\gamma_1 \neq \gamma_2$ (i.e., $m_1 \neq m_2$). Should the material be degenerate with isotropy being a special case, one only needs to slightly perturb the material properties to distinguish γ_1 and γ_2 (and thus m_1 and m_2) (Pan, 1997). The solutions thus obtained for a nearly isotropic material can still be verified against the isotropic solutions of Okada (1985, 1992), as will be shown below in the Numerical Examples section.

Point-Source Solutions in a Transversely Isotropic Half-Space

We first derive the point-force Green's tensor $u_{ij}(\mathbf{y};\mathbf{x})$, which denotes the ith component of the displacement vector at $\mathbf{y}(y_1,y_2,y_3)$ due to a unit point force in the jth direction applied at $\mathbf{x}(x_1,x_2,x_3)$ in a transversely isotropic half-space. Using the image method, this Green's tensor can be expressed in terms of a simple superposition of two individual parts as

$$
u_{ij}(\mathbf{y};\mathbf{x}) = u_{ij}^{\infty}(\mathbf{y};\mathbf{x})+u_{ij}^{c}(\mathbf{y};\mathbf{x}), \qquad (5)
$$

in which $u_{ij}^{\infty}(\mathbf{y};\mathbf{x})$ is the point-force Green's tensor of a transversely isotropic full-space, whereas $u_{ij}^{c}(\mathbf{y};\mathbf{x})$ is the complementary part from the image source due to the free surface of the half-space. They can be expressed in a new, simple, and unified way as

$$
\begin{aligned}
\begin{Bmatrix} u_{ij}^{\infty}(\mathbf{y};\mathbf{x}) \\ u_{ij}^{c}(\mathbf{y};\mathbf{x}) \end{Bmatrix} &= \frac{1}{4\pi c_{44}}\frac{\partial^2}{\partial y_i \partial x_j}\begin{Bmatrix} \Psi_{ij}^{\infty}(\mathbf{y};\mathbf{x}) \\ \Psi_{ij}^{c}(\mathbf{y};\mathbf{x}) \end{Bmatrix}\\
&+\frac{\delta_{ij}}{4\pi c_{44}}\frac{\partial^2}{\partial x_3^2}\begin{Bmatrix} \Phi_{i}^{\infty}(\mathbf{y};\mathbf{x}) \\ \Phi_{i}^{c}(\mathbf{y};\mathbf{x}) \end{Bmatrix} \qquad (6)
\end{aligned}
$$

(see Yuan, Pan, and Chen, 2013), in which

$$
\begin{aligned}
&\begin{Bmatrix} \Psi_{\xi\eta}^{\infty}(\mathbf{y};\mathbf{x}) \\ \Psi_{\xi\eta}^{c}(\mathbf{y};\mathbf{x}) \end{Bmatrix} = \begin{Bmatrix} \psi_1^{\infty}(\mathbf{y};\mathbf{x})-\gamma_3\chi_3(\mathbf{y};\mathbf{x}) \\ \psi_1^{c}(\mathbf{y};\mathbf{x})-\gamma_3\chi_{33}(\mathbf{y};\mathbf{x}) \end{Bmatrix},\\
&\begin{Bmatrix} \Psi_{3\eta}^{\infty}(\mathbf{y};\mathbf{x}) \\ \Psi_{3\eta}^{c}(\mathbf{y};\mathbf{x}) \end{Bmatrix} = \begin{Bmatrix} \psi_2^{\infty}(\mathbf{y};\mathbf{x}) \\ \psi_2^{c}(\mathbf{y};\mathbf{x}) \end{Bmatrix},\\
&\begin{Bmatrix} \Psi_{\xi 3}^{\infty}(\mathbf{y};\mathbf{x}) \\ \Psi_{\xi 3}^{c}(\mathbf{y};\mathbf{x}) \end{Bmatrix} = \begin{Bmatrix} \psi_3^{\infty}(\mathbf{y};\mathbf{x}) \\ \psi_3^{c}(\mathbf{y};\mathbf{x}) \end{Bmatrix},\\
&\begin{Bmatrix} \Psi_{33}^{\infty}(\mathbf{y};\mathbf{x}) \\ \Psi_{33}^{c}(\mathbf{y};\mathbf{x}) \end{Bmatrix} = \begin{Bmatrix} \psi_4^{\infty}(\mathbf{y};\mathbf{x}) \\ \psi_4^{c}(\mathbf{y};\mathbf{x}) \end{Bmatrix}, \qquad (7a)
\end{aligned}
$$

and

$$
\begin{Bmatrix} \Phi_{\xi}^{\infty}(\mathbf{y};\mathbf{x}) \\ \Phi_{\xi}^{c}(\mathbf{y};\mathbf{x}) \end{Bmatrix} = \begin{Bmatrix} \gamma_3^3\chi_3(\mathbf{y};\mathbf{x}) \\ \gamma_3^3\chi_{33}(\mathbf{y};\mathbf{x}) \end{Bmatrix}, \qquad \begin{Bmatrix} \Phi_{3}^{\infty}(\mathbf{y};\mathbf{x}) \\ \Phi_{3}^{c}(\mathbf{y};\mathbf{x}) \end{Bmatrix} = \begin{Bmatrix} 0 \\ 0 \end{Bmatrix}. \qquad (7b)
$$

The functions in equations (6), (7a), and (7b) are defined as

$$
\begin{aligned}
\psi_q^{\infty}(\mathbf{y};\mathbf{x}) &= \frac{1}{\Theta}\frac{(-1)^{\beta}}{\gamma_1-\gamma_2}T_{\beta}^{q}\chi_{\beta}(\mathbf{y};\mathbf{x}),\\
\psi_q^{c}(\mathbf{y};\mathbf{x}) &= \frac{1}{\Theta}\frac{(-1)^{\alpha+\beta+1}\mathrm{P}_{\alpha\beta}}{(\gamma_1-\gamma_2)^2\Lambda}T_{\alpha\beta}^{q}\chi_{\alpha\beta}(\mathbf{y};\mathbf{x}) \qquad (q=1,2,3,4) \qquad (8)
\end{aligned}
$$

(see Ding *et al.*, 2006; Yuan, Pan, and Chen, 2013), in which

$$
\begin{aligned}
&T_{\beta}^{1}=\gamma_\beta/m_\beta, \qquad T_{\beta}^{2}=T_{\beta}^{3}=\gamma_\beta, \qquad T_{\beta}^{4}=m_\beta\gamma_\beta,\\
&T_{\alpha\beta}^{1}=\gamma_\beta/m_\beta, \qquad T_{\alpha\beta}^{2}=m_\alpha\gamma_\beta/m_\beta, \qquad T_{\alpha\beta}^{3}=\gamma_\beta,\\
&T_{\alpha\beta}^{4}=m_\alpha\gamma_\beta, \qquad (9)
\end{aligned}
$$

and

$$
\begin{aligned}
\Lambda &= s_1 s_2(m_1+m_2+2),\\
\mathrm{P}_{\alpha\beta} &= -(m_{3-\alpha}+1)(m_\beta+1)(s_{3-\alpha}+s_\beta). \qquad (10)
\end{aligned}
$$

The potential functions χ_j and χ_{ij} in equations (7a), (7b), and (8) are defined as

$$\chi_j(\mathbf{y};\mathbf{x})\equiv\chi_j = \begin{cases} +z_j\ln(R_j+z_j)-R_j & \text{if } R_j+z_j\neq 0 \\ -z_j\ln(R_j-z_j)-R_j & \text{if } R_j+z_j=0 \end{cases}$$
$$\chi_{ij}(\mathbf{y};\mathbf{x})\equiv\chi_{ij} = -z_{ij}\ln(R_{ij}-z_{ij})-R_{ij} \tag{11}$$

(see Fabrikant, 2004; Ding *et al.*, 2006), in which

$$R_j = R_j(\mathbf{y};\mathbf{x}) = \sqrt{(y_1-x_1)^2+(y_2-x_2)^2+(z_j)^2},$$
$$R_{ij} = R_{ij}(\mathbf{y};\mathbf{x}) = \sqrt{(y_1-x_1)^2+(y_2-x_2)^2+(z_{ij})^2}, \tag{12}$$

and

$$z_j = z_j(\mathbf{y};\mathbf{x}) = s_j(y_3-x_3),$$
$$z_{ij} = z_{ij}(\mathbf{y};\mathbf{x}) = s_i y_3 + s_j x_3. \tag{13}$$

We point out that the above point-force solutions are extremely simple, involving only the scaled distances between the source and field points R_j and R_{ij} and the natural logarithmic function ln( ), as defined in equation (11).

Based on these point-force solutions, we now present the corresponding point-dislocation solution. We consider an infinitesimal surface of area dA with an arbitrary orientation in a transversely isotropic half-space. An infinitesimal dislocation is created by displacing the lower surface of dA by the Burgers vector $\mathbf{b}(b_1,b_2,b_3)$ relative to its upper surface and then rejoining the lower and upper surfaces together. We define the positive normal $\mathbf{n}(n_1,n_2,n_3)$ of the infinitesimal surface as the outward normal of the lower surface (Pan, 1991); then the positive direction of the closed dislocation curve surrounding the infinitesimal surface is determined by the positive normal $\mathbf{n}$ according to the right-hand rule (Yuan, Chen, and Pan, 2013). Using Betti's reciprocal theorem (see Pan, 1989), the point-dislocation solution in a transversely isotropic half-space can be found simply as

$$u_m^{ij}(\mathbf{x};\mathbf{y}) = -c_{ijkl}\frac{\partial}{\partial y_l}u_{km}(\mathbf{y};\mathbf{x}), \tag{14}$$

in which $u_m^{ij}(\mathbf{x};\mathbf{y})$ is the mth component of the displacement vector at $\mathbf{x}(x_1,x_2,x_3)$ due to an infinitesimal dislocation of unit area located at $\mathbf{y}(y_1,y_2,y_3)$ with positive normal component along $\mathbf{e}_i$ and Burgers vector component along $\mathbf{e}_j$. Here, $\mathbf{e}_i(i=1,2,3)$ is the unit base vector of the global Cartesian coordinate system. It is noted that, except for the minus sign, the right side of equation (14) is actually the Green's stress tensor with components (ij) at $\mathbf{y}(y_1,y_2,y_3)$ due to a unit point force in the mth direction applied at $\mathbf{x}(x_1,x_2,x_3)$ (Pan, 1991).

Finite-Dislocation Solutions in a Transversely Isotropic Half-Space

We now assume a three-dimensional dislocation loop C of arbitrary shape with Burgers vector $\mathbf{b}(b_1,b_2,b_3)$, which bounds a curved surface A in a transversely isotropic half-space. We point out that the polygonal dislocation surface $ABCDE$ shown in Figure 1 is a simple example. By integrating the point-dislocation solution in equation (14) over the curved surface A, the elastic displacement field induced by the loop C can be expressed as

$$u_m(\mathbf{x}) = \int_A \mathrm{d}A_i b_j u_m^{ij}(\mathbf{x};\mathbf{y}) \tag{15}$$

(see Hirth and Lothe, 1982; Yuan, Chen, and Pan, 2013; Yuan, Pan, and Chen, 2013), in which $u_m(\mathbf{x})$ is the mth component of the displacement vector at $\mathbf{x}(x_1,x_2,x_3)$ due to the dislocation loop in the half-space, and $\mathrm{d}A_i(=n_i\mathrm{d}A)$ is the ith component of the area element vector d$\mathbf{A}$ at $\mathbf{y}(y_1,y_2,y_3)$.

The area integral in equation (15) can be transformed into a line integral form as follows (see Yuan, Pan, and Chen, 2013):

$$u_m(\mathbf{x}) = u_m^{\infty}(\mathbf{x}) + u_m^{c}(\mathbf{x}), \tag{16}$$

in which

$$\begin{Bmatrix} u_m^{\infty}(\mathbf{x}) \\ u_m^{c}(\mathbf{x}) \end{Bmatrix} = -\frac{b_m}{4\pi}\begin{Bmatrix} \Omega_3^{\infty}(\mathbf{x}) \\ \Omega_{m;33}^{c}(\mathbf{x}) \end{Bmatrix} - \frac{1}{4\pi}\oint_C b_j\varepsilon_{mjk}\mathrm{d}y_k\begin{Bmatrix} W_{m;j}^{\infty}(\mathbf{y};\mathbf{x}) \\ W_{m;j}^{c}(\mathbf{y};\mathbf{x}) \end{Bmatrix}$$
$$-\frac{1}{4\pi}\frac{\partial}{\partial x_m}\oint_C b_j\varepsilon_{ijk}\mathrm{d}y_k\frac{\partial}{\partial y_i}\begin{Bmatrix} W_{m;ij}^{\infty}(\mathbf{y};\mathbf{x}) \\ W_{m;ij}^{c}(\mathbf{y};\mathbf{x}) \end{Bmatrix}. \tag{17}$$

In equation (17), the subscript semicolon is used to separate the subscript groups, and ε_{ijk} is the permutation symbol. Also in equation (17), we define

$$\Omega_3^{\infty}(\mathbf{x}) = \int_A\left(\mathrm{d}A_\xi\frac{\partial}{\partial y_\xi}+\gamma_3^2\mathrm{d}A_3\frac{\partial}{\partial y_3}\right)\frac{1}{\gamma_3 R_3},$$
$$\Omega_{\beta;33}^{c}(\mathbf{x}) = \oint_C\varepsilon_{i3k}\mathrm{d}y_k\frac{\partial^2}{\partial y_i\partial y_3}\gamma_3\chi_{33},$$
$$\Omega_{3;33}^{c}(\mathbf{x}) = -\oint_C\varepsilon_{i3k}\mathrm{d}y_k\frac{\partial^2}{\partial y_i\partial y_3}\gamma_3\chi_{33}, \tag{18a}$$

$$\begin{Bmatrix} W_{\beta;\xi}^{\infty}(\mathbf{y};\mathbf{x}) \\ W_{\beta;\xi}^{c}(\mathbf{y};\mathbf{x}) \end{Bmatrix} = \frac{\partial^2}{\partial y_3^2}\begin{Bmatrix} \gamma_3\chi_3 \\ \gamma_3\chi_{33} \end{Bmatrix},$$
$$\begin{Bmatrix} W_{\beta;3}^{\infty}(\mathbf{y};\mathbf{x}) \\ W_{\beta;3}^{c}(\mathbf{y};\mathbf{x}) \end{Bmatrix} = \gamma_3^2\frac{\partial^2}{\partial y_3^2}\begin{Bmatrix} \gamma_3\chi_3 \\ \gamma_3\chi_{33} \end{Bmatrix},$$
$$\begin{Bmatrix} W_{3;\xi}^{\infty}(\mathbf{y};\mathbf{x}) \\ W_{3;\xi}^{c}(\mathbf{y};\mathbf{x}) \end{Bmatrix} = -\frac{\partial^2}{\partial x_3\partial y_3}\begin{Bmatrix} \gamma_3\chi_3 \\ \gamma_3\chi_{33} \end{Bmatrix},$$
$$\begin{Bmatrix} W_{3;3}^{\infty}(\mathbf{y};\mathbf{x}) \\ W_{3;3}^{c}(\mathbf{y};\mathbf{x}) \end{Bmatrix} = -\gamma_3^2\frac{\partial^2}{\partial x_3\partial y_3}\begin{Bmatrix} \gamma_3\chi_3 \\ \gamma_3\chi_{33} \end{Bmatrix}, \tag{18b}$$

$$\begin{Bmatrix} W^{\infty}_{\beta;\xi\eta}(\mathbf{y};\mathbf{x}) \\ W^{c}_{\beta;\xi\eta}(\mathbf{y};\mathbf{x}) \end{Bmatrix} = 2s_3^2 \begin{Bmatrix} \psi_1^{\infty} - \gamma_3\chi_3 \\ \psi_1^{c} - \gamma_3\chi_{33} \end{Bmatrix},$$
$$\begin{Bmatrix} W^{\infty}_{\beta;j3}(\mathbf{y};\mathbf{x}) \\ W^{c}_{\beta;j3}(\mathbf{y};\mathbf{x}) \end{Bmatrix} = \begin{Bmatrix} W^{\infty}_{\beta;3j}(\mathbf{y};\mathbf{x}) \\ W^{c}_{\beta;3j}(\mathbf{y};\mathbf{x}) \end{Bmatrix} = \begin{Bmatrix} \psi_1^{\infty} + \psi_2^{\infty} - \gamma_3\chi_3 \\ \psi_1^{c} + \psi_2^{c} - \gamma_3\chi_{33} \end{Bmatrix},$$
$$\begin{Bmatrix} W^{\infty}_{3;\xi\eta}(\mathbf{y};\mathbf{x}) \\ W^{c}_{3;\xi\eta}(\mathbf{y};\mathbf{x}) \end{Bmatrix} = 2s_3^2 \begin{Bmatrix} \psi_3^{\infty} \\ \psi_3^{c} \end{Bmatrix},$$
$$\begin{Bmatrix} W^{\infty}_{3;j3}(\mathbf{y};\mathbf{x}) \\ W^{c}_{3;j3}(\mathbf{y};\mathbf{x}) \end{Bmatrix} = \begin{Bmatrix} W^{\infty}_{3;3j}(\mathbf{y};\mathbf{x}) \\ W^{c}_{3;3j}(\mathbf{y};\mathbf{x}) \end{Bmatrix} = \begin{Bmatrix} \psi_3^{\infty} + \psi_4^{\infty} + \gamma_3\chi_3 \\ \psi_3^{c} + \psi_4^{c} + \gamma_3\chi_{33} \end{Bmatrix}. \tag{18c}$$

The line integrals in equation (17) are along the positive direction of the closed dislocation loop C. The area integral $\Omega_3^{\infty}(\mathbf{x})$ shown in equation (18a) is the quasi-solid angle subtended by the cut surface of the dislocation loop at point $\mathbf{x}$ in the transversely isotropic full-space, which can also be transformed into a line integral (see Yuan, Chen, and Pan, 2013).

We now let $U_{ij}(\mathbf{x})$ denote the ith component of the displacement vector at $\mathbf{x}(x_1, x_2, x_3)$ due to a dislocation loop in the half-space with unit Burgers vector in the jth direction. Then $U_{ij}(\mathbf{x})$ can be expressed as

$$U_{ij}(\mathbf{x}) = U^{\infty}_{ij}(\mathbf{x}) + U^{c}_{ij}(\mathbf{x}), \tag{19}$$

in which $U^{\infty}_{ij}(\mathbf{x})$ denotes the ith component of the displacement vector at $\mathbf{x}(x_1, x_2, x_3)$ due to a dislocation loop in the corresponding full-space with the unit Burgers vector in the jth direction, and $U^{c}_{ij}(\mathbf{x})$ accounts for the influence of the free surface of the half-space. Although all components in $U_{ij}(\mathbf{x})$ can be directly obtained from equation (17), we modify $U_{\beta 3}(\mathbf{x})$ slightly for the benefit of further simplifications. From equation (17) we have

$$4\pi \begin{Bmatrix} U^{\infty}_{\beta 3}(\mathbf{x}) \\ U^{c}_{\beta 3}(\mathbf{x}) \end{Bmatrix} = -\oint_C \varepsilon_{\beta 3\xi} \mathrm{d}y_\xi \gamma_3^2 \frac{\partial^2}{\partial y_3^2} \begin{Bmatrix} \psi_0^{\infty} \\ \psi_0^{c} \end{Bmatrix} - \frac{\partial}{\partial x_\beta} \oint_C \varepsilon_{\alpha 3\eta} \mathrm{d}y_\eta \frac{\partial}{\partial y_\alpha} \begin{Bmatrix} \psi_1^{\infty} + \psi_2^{\infty} - \psi_0^{\infty} \\ \psi_1^{c} + \psi_2^{c} - \psi_0^{c} \end{Bmatrix}. \tag{20}$$

Then, by utilizing the following relation

$$\begin{aligned} &\oint_C \varepsilon_{\alpha 3\eta} \mathrm{d}y_\eta \frac{\partial^2}{\partial y_\beta \partial y_\alpha} \begin{Bmatrix} \psi_1^{\infty} + \psi_2^{\infty} - \psi_0^{\infty} \\ \psi_1^{c} + \psi_2^{c} - \psi_0^{c} \end{Bmatrix} \\ &= \oint_C \varepsilon_{\alpha\beta 3} \mathrm{d}y_3 \frac{\partial^2}{\partial y_3 \partial y_\alpha} \begin{Bmatrix} \psi_1^{\infty} + \psi_2^{\infty} - \psi_0^{\infty} \\ \psi_1^{c} + \psi_2^{c} - \psi_0^{c} \end{Bmatrix} \\ &+ \oint_C \varepsilon_{\beta 3\xi} \mathrm{d}y_\xi \frac{\partial^2}{\partial y_\alpha^2} \begin{Bmatrix} \psi_1^{\infty} + \psi_2^{\infty} - \psi_0^{\infty} \\ \psi_1^{c} + \psi_2^{c} - \psi_0^{c} \end{Bmatrix}, \end{aligned} \tag{21}$$

equation (20) can be transformed into

$$4\pi \begin{Bmatrix} U^{\infty}_{\beta 3}(\mathbf{x}) \\ U^{c}_{\beta 3}(\mathbf{x}) \end{Bmatrix} = \oint_C \varepsilon_{\beta 3\xi} \mathrm{d}y_\xi \frac{\partial^2}{\partial y_\alpha^2} \begin{Bmatrix} \psi_1^{\infty} + \psi_2^{\infty} \\ \psi_1^{c} + \psi_2^{c} \end{Bmatrix} + \oint_C \varepsilon_{\alpha\beta 3} \mathrm{d}y_3 \frac{\partial}{\partial y_3} \frac{\partial}{\partial y_\alpha} \begin{Bmatrix} \psi_1^{\infty} + \psi_2^{\infty} - \psi_0^{\infty} \\ \psi_1^{c} + \psi_2^{c} - \psi_0^{c} \end{Bmatrix}. \tag{22}$$

With these preparations, we can now express the dislocation-loop-induced fields in terms of simple line integrals along the loop with the integrands being elementary functions. We point out that, in this article, the dislocation loop C is called simple if one of the following conditions is satisfied: (I) the dislocation surface A is described by a single-valued function $x_3 = S(x_1, x_2)$ or (II) the dislocation surface A coincides with a certain cylindrical surface perpendicular to the x_1–x_2 plane. Actually, condition (II) can be considered as a limiting case of condition (I), and a general loop can always be divided into certain simple ones (see Yuan, Chen, and Pan, 2013). Because of the above facts and without loss of generality, we now express $U_{ij}(\mathbf{x})$ explicitly for a simple dislocation loop C under condition (I). Furthermore, we order them first by the full-space solution and then followed by the complementary part.

$$4\pi(-1)^{\xi} U^{\infty}_{\xi\xi}(\mathbf{x}) = (-1)^{\xi}(-\Omega_3^{\infty}) - g_i s_i \mathrm{I}^{\xi 3}_{2;i;(3-\xi)} - 2s_3^2 f_i \gamma_i \mathrm{C}_i^{12}, \tag{23a}$$

$$4\pi(-1)^{\xi} U^{\infty}_{\xi(3-\xi)}(\mathbf{x}) = s_3 \mathrm{I}^{\sim}_{0;3;3} + g_i s_i \mathrm{I}^{\xi 3}_{2;i;\xi} - 2s_3^2 f_i \gamma_i \mathrm{C}_i + 2s_3^2 f_i \gamma_i \mathrm{C}_i^{\xi\xi}, \tag{23b}$$

$$4\pi(-1)^{\xi} U^{\infty}_{3(3-\xi)}(\mathbf{x}) = -m_\beta s_\beta (2s_3^2 f_\beta \mathrm{I}^{\xi 3}_{2;\beta;3} + g_\beta \mathrm{I}^{\sim}_{0;\beta;\xi}), \tag{23c}$$

$$4\pi(-1)^{\xi} U^{\infty}_{(3-\xi)3}(\mathbf{x}) = -g_i s_i \mathrm{I}^{\xi 3}_{2;i;3} - g_\alpha \gamma_\alpha \mathrm{I}^{\sim}_{0;\alpha;\xi}, \tag{23d}$$

$$4\pi U^{\infty}_{33}(\mathbf{x}) = \mathrm{sgn}\langle S(x_1, x_2) - x_3 \rangle \bar{\mathrm{C}} + m_\beta g_\beta s_\beta \mathrm{C}^{-}_{\beta}, \tag{23e}$$

$$4\pi(-1)^{\xi} U^{c}_{\xi\xi}(\mathbf{x}) = (-1)^{\xi}(-\bar{\mathrm{C}} + s_3 \mathrm{C}^{-}_{33}) - g_{ij} s_i \mathrm{I}^{\xi 3}_{2;ij;(3-\xi)} - 2s_3^2 f_{ij} \gamma_i \mathrm{C}_{ij}^{12} - 4s_3^2 f_{ij} \mathrm{L}^{123}_{4;ij;3}, \tag{24a}$$

$$4\pi(-1)^{\xi} U^{c}_{\xi(3-\xi)}(\mathbf{x}) = s_3 \mathrm{I}^{\sim}_{0;33;3} + g_{ij} s_i \mathrm{I}^{\xi 3}_{2;ij;\xi} - 2s_3^2 f_{ij} \gamma_i \mathrm{C}_{ij} + 2s_3^2 f_{ij} \gamma_i \mathrm{C}_{ij}^{\xi\xi} + 2s_3^2 f_{ij} \bar{\mathrm{C}}_{ij}^{\xi}, \tag{24b}$$

$$4\pi(-1)^{\xi} U^{c}_{3(3-\xi)}(\mathbf{x}) = m_\beta s_\beta (2s_3^2 f_{\alpha\beta} \mathrm{I}^{\xi 3}_{2;\alpha\beta;3} + g_{\alpha\beta} \mathrm{I}^{\sim}_{0;\alpha\beta;\xi}) + 2s_3^2 F \mathrm{L}^{\xi}_{2;\sim;3}, \tag{24c}$$

$$4\pi(-1)^{\xi}U^{c}_{(3-\xi)3}(\mathbf{x}) = -g_{ij}s_i\mathrm{I}^{\xi 3}_{2;ij;3} - g_{\alpha\beta}\gamma_\alpha\mathrm{I}^{\sim}_{0;\alpha\beta;\xi}, \tag{24d}$$

$$4\pi U^{c}_{33}(\mathbf{x}) = -\bar{\mathrm{C}} - m_\beta g_{\alpha\beta}s_\beta\mathrm{C}^{-}_{\alpha\beta}. \tag{24e}$$

In equations (23) and (24), $\mathrm{sgn}\langle x\rangle$ is the sign function, and

$$\begin{aligned}\mathrm{C}^{\eta\xi}_{i}(\mathbf{x}) &= 2s_i^2\mathrm{I}^{\eta\xi 33}_{4;i;3}(\mathbf{x}) + \mathrm{I}^{\eta\xi}_{2;i;3}(\mathbf{x}),\\ \mathrm{C}^{\eta\xi}_{i}(\mathbf{x}) &= 2s_i^2\mathrm{I}^{\eta\xi 33}_{4;ij;3}(\mathbf{x}) + \mathrm{I}^{\eta\xi}_{2;ij;3}(\mathbf{x}),\end{aligned} \tag{25a}$$

$$\begin{aligned}\mathrm{C}^{-}_{i}(\mathbf{x}) &= \mathrm{I}^{23}_{2;i;1}(\mathbf{x}) - \mathrm{I}^{13}_{2;i;2}(\mathbf{x}),\\ \mathrm{C}^{-}_{ij}(\mathbf{x}) &= \mathrm{I}^{23}_{2;ij;1}(\mathbf{x}) - \mathrm{I}^{13}_{2;ij;2}(\mathbf{x}),\end{aligned} \tag{25b}$$

$$\begin{aligned}\mathrm{C}_{i}(\mathbf{x}) &= s_i^2\mathrm{I}^{33}_{2;i;3}(\mathbf{x}) + \mathrm{I}^{\sim}_{0;i;3}(\mathbf{x}),\\ \mathrm{C}_{ij}(\mathbf{x}) &= s_i^2\mathrm{I}^{33}_{2;ij;3}(\mathbf{x}) + \mathrm{I}^{\sim}_{0;ij;3}(\mathbf{x}),\end{aligned} \tag{25c}$$

$$\begin{aligned}\bar{\mathrm{C}}(\mathbf{x}) &= \mathrm{L}^{1}_{2;\sim;2}(\mathbf{x}) - \mathrm{L}^{2}_{2;\sim;1}(\mathbf{x}),\\ \bar{\mathrm{C}}^{\xi}_{ij}(\mathbf{x}) &= 2\mathrm{L}^{\xi\xi 3}_{4;ij;3}(\mathbf{x}) - \mathrm{L}^{3}_{2;ij;3}(\mathbf{x}),\\ \Omega^{\infty}_{3}(\mathbf{x}) &= -\mathrm{sgn}\langle S(x_1,x_2)-x_3\rangle\bar{\mathrm{C}}(\mathbf{x}) - s_3\mathrm{C}^{-}_{3}(\mathbf{x}).\end{aligned} \tag{25d}$$

We point out that the difference between the three function pairs $\mathrm{C}^{\eta\xi}_{i}(\mathbf{x})$ and $\mathrm{C}^{\eta\xi}_{ij}(\mathbf{x})$ in equation (25a), $\mathrm{C}^{-}_{i}(\mathbf{x})$ and $\mathrm{C}^{-}_{ij}(\mathbf{x})$ in equation (25b), and $\mathrm{C}_{i}(\mathbf{x})$ and $\mathrm{C}_{ij}(\mathbf{x})$ in equation (25c) is that the latter expression in each pair can be obtained directly from the former one by replacing the subscript i in the former function $\mathrm{I}_{*;\mathrm{I};*}(\mathbf{x})$ by subscripts ij to become $\mathrm{I}_{*;ij;*}(\mathbf{x})$. This is equivalent to replacing x_3 by x_3^{ij} defined in equation (27) below. In other words, once we have the exact closed-form expressions for the former functions, we can obtain the exact closed-form expressions for the latter functions by simply replacing x_3 by x_3^{ij} in the former expressions. This becomes apparent by looking at the definitions of the involved functions $\mathrm{I}(\mathbf{x})$, $\mathrm{L}(\mathbf{x})$, and $\mathrm{J}(\mathbf{x})$ below.

$$\begin{aligned}\mathrm{I}^{\sim}_{0;i;k}(x_1,x_2,x_3) &= \oint_C\frac{1}{R_i}\mathrm{d}y_k,\\ \mathrm{I}^{\sim}_{0;ij;k}(x_1,x_2,x_3) &\equiv \mathrm{I}^{\sim}_{0;\sim;k}(x_1,x_2,x_3^{ij}) = \oint_C\frac{1}{R_{ij}}\mathrm{d}y_k,\end{aligned} \tag{26a}$$

$$\begin{aligned}\mathrm{I}^{\xi 3\cdots}_{N;i;k}(x_1,x_2,x_3) &= \oint_C\frac{(y_\xi-x_\xi)(y_3-x_3)\cdots}{\bar{R}^N R_i}\mathrm{d}y_k,\\ \mathrm{I}^{\xi 3\cdots}_{N;ij;k}(x_1,x_2,x_3) &\equiv \mathrm{I}^{\xi 3\cdots}_{N;\sim;k}(x_1,x_2,x_3^{ij})\\ &= \oint_C\frac{(y_\xi-x_\xi)(\gamma_i z_{ij})\cdots}{\bar{R}^N R_{ij}}\mathrm{d}y_k,\end{aligned} \tag{26b}$$

$$\begin{aligned}\mathrm{L}^{\xi 3\cdots}_{N;\sim;k}(x_1,x_2,x_3) &= \oint_C\frac{(y_\xi-x_\xi)(y_3-x_3)\cdots}{\bar{R}^N}\mathrm{d}y_k,\\ \mathrm{L}^{\xi 3\cdots}_{N;ij;k}(x_1,x_2,x_3) &\equiv \mathrm{L}^{\xi 3\cdots}_{N;\sim;k}(x_1,x_2,x_3^{ij})\\ &= \oint_C\frac{(y_\xi-x_\xi)(\gamma_i z_{ij})\cdots}{\bar{R}^N}\mathrm{d}y_k,\end{aligned} \tag{26c}$$

$$\begin{aligned}\mathrm{J}^{\xi 3\cdots}_{N;i;k}(x_1,x_2,x_3) &= \oint_C\frac{(y_\xi-x_\xi)(y_3-x_3)\cdots}{\bar{R}^N R_i^3}\mathrm{d}y_k,\\ \mathrm{J}^{\xi 3\cdots}_{N;ij;k}(x_1,x_2,x_3) &\equiv \mathrm{J}^{\xi 3\cdots}_{N;\sim;k}(x_1,x_2,x_3^{ij})\\ &= \oint_C\frac{(y_\xi-x_\xi)(\gamma_i z_{ij})\cdots}{\bar{R}^N R_{ij}^3}\mathrm{d}y_k,\end{aligned} \tag{26d}$$

in which N is an even number and

$$\bar{R} = \sqrt{(y_1-x_1)^2+(y_2-x_2)^2}, \qquad x_3^{ij} = -\gamma_i s_j x_3. \tag{27}$$

Again, the paired function relation discussed above can be clearly observed from equations (26a), (26b), and (26d), in which R_i is involved in the integrand. We point out that the function $\mathrm{J}(\mathbf{x})$ defined in equation (26d) will occur in later derivations (e.g., in equations 30a–h and 31a–h). We also remark, in some special cases, the line integrals in equation (26) become divergent so that they should be integrated in the finite-part sense.

We further point out that, in equations (23) and (24), although equations (23d) and (24d) are derived from equation (22), equations (23a)–(23c), (23e), (24a)–(24c), and (24e) are all derived from equation (17). Also in equations (23) and (24), the coefficients are defined as

$$\begin{aligned}f_\alpha &= \frac{(-1)^{\alpha+1}m_{3-\alpha}}{m_1-m_2}, \quad g_\alpha = (m_\alpha+1)f_\alpha, \quad f_3 = g_3 = 1,\\ f_{\alpha\beta} &= \frac{(-1)^{\alpha+\beta+1}(m_{3-\alpha}+1)(m_{3-\beta}+1)(\gamma_{3-\alpha}+\gamma_\beta)}{\Theta(m_1+m_2+2)(\gamma_1-\gamma_2)^2},\\ g_{\alpha\beta} &= (m_\alpha+1)f_{\alpha\beta}, \quad f_{33} = g_{33} = 1, \quad f_{\alpha 3} = g_{\alpha 3} = 0,\\ f_{3\beta} &= g_{3\beta} = 0, \qquad F = \frac{\Theta(\gamma_1+\gamma_2)}{(m_1+m_2+2)} - 1.\end{aligned} \tag{28}$$

Note that when deriving equations (23) and (24), use has been made of the following relations:

$$\begin{aligned}&\sum_i f_i = 0, \quad \sum_i g_i = 0, \quad 1+\sum_\alpha\sum_\beta g_{\alpha\beta} = 0,\\ &\sum_\alpha\sum_\beta (m_\beta+1)g_{\alpha\beta} = 0, \quad 1+\sum_\alpha\sum_\beta (m_\beta+1)s_\beta\gamma_\alpha f_{\alpha\beta} = 0.\end{aligned} \tag{29}$$

We remark that, instead of taking derivatives of the displacement solutions, the distortions can also be calculated directly from equations (17) and (22) as follows:

$$4\pi(-1)^{\xi}\frac{\partial U^{\infty}_{\eta(3-\xi)}(\mathbf{x})}{\partial x_{\tau}} = \varepsilon_{\eta\xi 3}(-1)^{\tau}s_3(\mathrm{J}^3_{0;3;(3-\tau)} - \mathrm{J}^{(3-\tau)}_{0;3;3}) + \delta_{\eta\xi}s_3\mathrm{J}^{\tau}_{0;3;3} + g_i s_i \mathrm{C}^{\eta\tau}_{i;\xi} + 2s_3^2 f_i\gamma_i \mathrm{C}^{\eta\xi\tau}_{i}, \tag{30a}$$

$$4\pi(-1)^{\xi}\frac{\partial U^{\infty}_{\eta(3-\xi)}(\mathbf{x})}{\partial x_{3}} = \delta_{\eta\xi}s_3^3\mathrm{J}^3_{0;3;3} - s_3\mathrm{J}^{\xi}_{0;3;\eta} - g_\beta s_\beta \mathrm{J}^{\eta}_{0;\beta;\xi} - 2s_3^2 f_j s_j \mathrm{C}^{\eta\xi}_{j;3}, \tag{30b}$$

$$4\pi(-1)^{\xi}\frac{\partial U^{\infty}_{3(3-\xi)}(\mathbf{x})}{\partial x_{\tau}} = -m_\beta g_\beta s_\beta \mathrm{J}^{\tau}_{0;\beta;\xi} - 2s_3^2 m_\beta f_\beta s_\beta \mathrm{C}^{\xi\tau}_{\beta;3}, \tag{30c}$$

$$4\pi(-1)^{\xi}\frac{\partial U^{\infty}_{3(3-\xi)}(\mathbf{x})}{\partial x_{3}} = -m_\beta s_\beta^2(g_\beta s_\beta \mathrm{J}^3_{0;\beta;\xi} - 2s_3^2 f_\beta\gamma_\beta \mathrm{J}^{\xi}_{0;\beta;3}), \tag{30d}$$

$$4\pi(-1)^{\xi}\frac{\partial U^{\infty}_{(3-\xi)3}(\mathbf{x})}{\partial x_{\tau}} = -g_\beta\gamma_\beta \mathrm{J}^{\tau}_{0;\beta;\xi} - g_i s_i \mathrm{C}^{\xi\tau}_{i;3}, \tag{30e}$$

$$4\pi(-1)^{\xi}\frac{\partial U^{\infty}_{(3-\xi)3}(\mathbf{x})}{\partial x_{3}} = -g_\beta s_\beta \mathrm{J}^3_{0;\beta;\xi} + g_i s_i \mathrm{J}^{\xi}_{0;i;3}, \tag{30f}$$

$$4\pi\frac{\partial U^{\infty}_{33}(\mathbf{x})}{\partial x_{\tau}} = -(-1)^{\tau}m_\beta g_\beta s_\beta(\mathrm{J}^{(3-\tau)}_{0;\beta;3} - \mathrm{J}^3_{0;\beta;(3-\tau)}), \tag{30g}$$

$$4\pi\frac{\partial U^{\infty}_{33}(\mathbf{x})}{\partial x_{3}} = m_\beta g_\beta s_\beta(\mathrm{J}^1_{0;\beta;2} - \mathrm{J}^2_{0;\beta;1}), \tag{30h}$$

$$4\pi(-1)^{\xi}\frac{\partial U^{\mathrm{c}}_{\eta(3-\xi)}(\mathbf{x})}{\partial x_{\tau}} = \varepsilon_{\eta\xi 3}(-1)^{\tau}s_3(\mathrm{J}^3_{0;33;(3-\tau)} - \mathrm{J}^{(3-\tau)}_{0;33;3}) + \delta_{\eta\xi}s_3\mathrm{J}^{\tau}_{0;33;3} + g_{ij}s_i\mathrm{C}^{\eta\tau}_{ij;\xi} + 2s_3^2 f_{ij}\gamma_i(\mathrm{C}^{\eta\xi\tau}_{ij} + 2s_i\bar{\mathrm{C}}^{\eta\xi\tau}_{ij}), \tag{31a}$$

$$4\pi(-1)^{\xi}\frac{\partial U^{\mathrm{c}}_{\eta(3-\xi)}(\mathbf{x})}{\partial x_{3}} = -\delta_{\eta\xi}s_3^3\mathrm{J}^3_{0;33;3} + s_3\mathrm{J}^{\xi}_{0;33;\eta} + g_{\alpha\beta}s_\beta\mathrm{J}^{\eta}_{0;\alpha\beta;\xi} + 2s_3^2(f_{ij}s_j\mathrm{C}^{\eta\xi}_{ij;3} - F\bar{\mathrm{C}}^{\eta\xi}), \tag{31b}$$

$$4\pi(-1)^{\xi}\frac{\partial U^{\mathrm{c}}_{3(3-\xi)}(\mathbf{x})}{\partial x_{\tau}} = m_\beta g_{\alpha\beta}s_\beta\mathrm{J}^{\tau}_{0;\alpha\beta;\xi} + 2s_3^2(m_\beta f_{\alpha\beta}s_\beta\mathrm{C}^{\xi\tau}_{\alpha\beta;3} + F\bar{\mathrm{C}}^{\xi\tau}), \tag{31c}$$

$$4\pi(-1)^{\xi}\frac{\partial U^{\mathrm{c}}_{3(3-\xi)}(\mathbf{x})}{\partial x_{3}} = -m_\beta s_\beta^2(g_{\alpha\beta}s_\alpha\mathrm{J}^3_{0;\alpha\beta;\xi} - 2s_3^2 f_{\alpha\beta}\gamma_\alpha\mathrm{J}^{\xi}_{0;\alpha\beta;3}), \tag{31d}$$

$$4\pi(-1)^{\xi}\frac{\partial U^{\mathrm{c}}_{(3-\xi)3}(\mathbf{x})}{\partial x_{\tau}} = -g_{\alpha\beta}\gamma_\alpha\mathrm{J}^{\tau}_{0;\alpha\beta;\xi} - g_{ij}s_i\mathrm{C}^{\xi\tau}_{ij;3}, \tag{31e}$$

$$4\pi(-1)^{\xi}\frac{\partial U^{\mathrm{c}}_{(3-\xi)3}(\mathbf{x})}{\partial x_{3}} = g_{\alpha\beta}s_\beta\mathrm{J}^3_{0;\alpha\beta;\xi} - g_{ij}s_j\mathrm{J}^{\xi}_{0;ij;3}, \tag{31f}$$

$$4\pi\frac{\partial U^{\mathrm{c}}_{33}(\mathbf{x})}{\partial x_{\tau}} = (-1)^{\tau}m_\beta g_{\alpha\beta}s_\beta(\mathrm{J}^{(3-\tau)}_{0;\alpha\beta;3} - \mathrm{J}^3_{0;\alpha\beta;(3-\tau)}), \tag{31g}$$

$$4\pi\frac{\partial U^{\mathrm{c}}_{33}(\mathbf{x})}{\partial x_{3}} = m_\beta g_{\alpha\beta}s_\beta s_\beta\gamma_\alpha(\mathrm{J}^1_{0;\alpha\beta;2} - \mathrm{J}^2_{0;\alpha\beta;1}), \tag{31h}$$

in which

$$\begin{aligned}\bar{\mathrm{C}}^{\eta\xi}(\mathbf{x}) &= 2\mathrm{L}^{\eta\xi}_{4;\sim;3}(\mathbf{x}) - \delta_{\eta\xi}\mathrm{L}^{\sim}_{2;\sim;3}(\mathbf{x})\\ \bar{\mathrm{C}}^{\eta\xi\tau}_{ij}(\mathbf{x}) &= 4\mathrm{L}^{\eta\xi\tau 3}_{6;ij;3}(\mathbf{x}) - \delta_{\eta\tau}\mathrm{L}^{\xi 3}_{4;ij;3}(\mathbf{x}) - \delta_{\xi\tau}\mathrm{L}^{\eta 3}_{4;ij;3}(\mathbf{x}) - \delta_{\eta\xi}\mathrm{L}^{\tau 3}_{4;ij;3}(\mathbf{x}),\end{aligned} \tag{32a}$$

$$\begin{aligned}\mathrm{C}^{\eta\xi}_{i;k}(\mathbf{x}) &= 2\mathrm{I}^{\eta\xi 3}_{4;i;k}(\mathbf{x}) + \mathrm{J}^{\eta\xi 3}_{2;i;k}(\mathbf{x}) - \delta_{\eta\xi}\mathrm{I}^{3}_{2;i;k}(\mathbf{x})\\ \mathrm{C}^{\eta\xi}_{ij;k}(\mathbf{x}) &= 2\mathrm{I}^{\eta\xi 3}_{4;ij;k}(\mathbf{x}) + \mathrm{J}^{\eta\xi 3}_{2;ij;k}(\mathbf{x}) - \delta_{\eta\xi}\mathrm{I}^{3}_{2;ij;k}(\mathbf{x}),\end{aligned} \tag{32b}$$

$$\begin{aligned}\mathrm{C}^{\eta\xi\tau}_{i}(\mathbf{x}) &= 8s_i^2\mathrm{I}^{\eta\xi\tau 33}_{6;i;3}(\mathbf{x}) + 4\mathrm{I}^{\eta\xi\tau}_{4;i;3}(\mathbf{x}) - \mathrm{J}^{\eta\xi\tau}_{2;i;3}(\mathbf{x})\\ &\quad - \delta_{\xi\tau}[2s_i^2\mathrm{I}^{\eta 33}_{4;i;3}(\mathbf{x}) + \mathrm{I}^{\eta}_{2;i;3}(\mathbf{x})]\\ &\quad - \delta_{\eta\xi}[2s_i^2\mathrm{I}^{\tau 33}_{4;i;3}(\mathbf{x}) + \mathrm{I}^{\tau}_{2;i;3}(\mathbf{x})]\\ &\quad - \delta_{\eta\tau}[2s_i^2\mathrm{I}^{\xi 33}_{4;i;3}(\mathbf{x}) + \mathrm{I}^{\xi}_{2;i;3}(\mathbf{x})],\\ \mathrm{C}^{\eta\xi\tau}_{ij}(\mathbf{x}) &= 8s_i^2\mathrm{I}^{\eta\xi\tau 33}_{6;ij;3}(\mathbf{x}) + 4\mathrm{I}^{\eta\xi\tau}_{4;ij;3}(\mathbf{x}) - \mathrm{J}^{\eta\xi\tau}_{2;ij;3}(\mathbf{x})\\ &\quad - \delta_{\xi\tau}[2s_i^2\mathrm{I}^{\eta 33}_{4;ij;3}(\mathbf{x}) + \mathrm{I}^{\eta}_{2;ij;3}(\mathbf{x})]\\ &\quad - \delta_{\eta\xi}[2s_i^2\mathrm{I}^{\tau 33}_{4;ij;3}(\mathbf{x}) + \mathrm{I}^{\tau}_{2;ij;3}(\mathbf{x})]\\ &\quad - \delta_{\eta\tau}[2s_i^2\mathrm{I}^{\xi 33}_{4;ij;3}(\mathbf{x}) + \mathrm{I}^{\xi}_{2;ij;3}(\mathbf{x})].\end{aligned} \tag{32c}$$

One observes that the functions defined in equations (32b) and (32c) are function pairs between their indexes i and ij, as discussed previously. We further note that while equations (30e), (30f), (31e), and (31f) are derived from equation (22), other distortion components in equations (30) and (31) are obtained from equation (17).

We also remark that when deriving the components involving the solid angle (referring to equations 18a and 23a), use has been made of the following relations (see Yuan, Chen, and Pan, 2013; Yuan, Pan, and Chen, 2013):

$$\frac{\partial \Omega_3^{\infty}(\mathbf{x})}{\partial x_\tau} = \oint_C \left(\varepsilon_{\tau\alpha k} \frac{\partial}{\partial y_\alpha} + \gamma_3^2 \varepsilon_{\tau 3 k} \frac{\partial}{\partial y_3} \right) \frac{1}{\gamma_3 R_3} \mathrm{d}y_k,$$
$$\frac{\partial \Omega_{1;33}^{\mathrm{c}}(\mathbf{x})}{\partial x_\tau} = \frac{\partial \Omega_{2;33}^{\mathrm{c}}(\mathbf{x})}{\partial x_\tau} = \oint_C \left(\varepsilon_{\tau\alpha k} \frac{\partial}{\partial y_\alpha} + \gamma_3^2 \varepsilon_{\tau 3 k} \frac{\partial}{\partial y_3} \right) \frac{1}{\gamma_3 R_{33}} \mathrm{d}y_k,$$
$$\frac{\partial \Omega_{3;33}^{\mathrm{c}}(\mathbf{x})}{\partial x_\tau} = -\oint_C \left(\varepsilon_{\tau\alpha k} \frac{\partial}{\partial y_\alpha} + \gamma_3^2 \varepsilon_{\tau 3 k} \frac{\partial}{\partial y_3} \right) \frac{1}{\gamma_3 R_{33}} \mathrm{d}y_k. \tag{33}$$

When deriving equations (30b) and (31b), use has been made of the following identity:

$$\delta_{\alpha\eta}\varepsilon_{\xi 3\beta} + \delta_{\alpha\xi}\varepsilon_{3\eta\beta} = -\delta_{\alpha\beta}\varepsilon_{\xi\eta 3}. \tag{34}$$

We finally point out that equations (23), (24), (30), and (31) are still applicable to a simple dislocation loop corresponding to condition (II), provided that we set the $\langle S(x_1, x_2) - x_3 \rangle$ term in equations (23a) and (23e) to be zero.

Polygonal-Source Solutions in a Transversely Isotropic Half-Space

We now consider a dislocation of polygonal shape lying within a general flat plane characterized by the two orientation angles ϕ and δ (Fig. 1). The strike-slip, dip-slip, and tensile components of the dislocation are denoted by U_{s}, U_{d}, and U_{t}, respectively (Fig. 1). Using the coordinate transformations, we can derive the induced (global) displacements and distortions as follows:

For a strike-slip fault,

$$\begin{aligned} u_i(\mathbf{x}) &= -U_s \cos\phi [U_{i1}^{\infty}(\mathbf{x}) + U_{i1}^{\mathrm{c}}(\mathbf{x})] \\ &\quad - U_s \sin\phi [U_{i2}^{\infty}(\mathbf{x}) + U_{i2}^{\mathrm{c}}(\mathbf{x})], \\ \frac{\partial u_i(\mathbf{x})}{\partial x_j} &= -U_s \cos\phi \left[\frac{\partial U_{i1}^{\infty}(\mathbf{x})}{\partial x_j} + \frac{\partial U_{i1}^{\mathrm{c}}(\mathbf{x})}{\partial x_j} \right] \\ &\quad - U_s \sin\phi \left[\frac{\partial U_{i2}^{\infty}(\mathbf{x})}{\partial x_j} + \frac{\partial U_{i2}^{\mathrm{c}}(\mathbf{x})}{\partial x_j} \right]. \end{aligned} \tag{35a}$$

For a dip-slip fault,

$$\begin{aligned} u_i(\mathbf{x}) &= U_d \sin\phi \cos\delta [U_{i1}^{\infty}(\mathbf{x}) + U_{i1}^{\mathrm{c}}(\mathbf{x})] \\ &\quad - U_d \cos\phi \cos\delta [U_{i2}^{\infty}(\mathbf{x}) + U_{i2}^{\mathrm{c}}(\mathbf{x})] \\ &\quad - U_d \sin\delta [U_{i3}^{\infty}(\mathbf{x}) + U_{i3}^{\mathrm{c}}(\mathbf{x})], \\ \frac{\partial u_i(\mathbf{x})}{\partial x_j} &= U_d \sin\phi \cos\delta \left[\frac{\partial U_{i1}^{\infty}(\mathbf{x})}{\partial x_j} + \frac{\partial U_{i1}^{\mathrm{c}}(\mathbf{x})}{\partial x_j} \right] \\ &\quad - U_d \cos\phi \cos\delta \left[\frac{\partial U_{i2}^{\infty}(\mathbf{x})}{\partial x_j} + \frac{\partial U_{i2}^{\mathrm{c}}(\mathbf{x})}{\partial x_j} \right] \\ &\quad - U_d \sin\delta \left[\frac{\partial U_{i3}^{\infty}(\mathbf{x})}{\partial x_j} + \frac{\partial U_{i3}^{\mathrm{c}}(\mathbf{x})}{\partial x_j} \right]. \end{aligned} \tag{35b}$$

For a tensile fracture,

$$\begin{aligned} u_i(\mathbf{x}) &= -U_t \sin\phi \sin\delta [U_{i1}^{\infty}(\mathbf{x}) + U_{i1}^{\mathrm{c}}(\mathbf{x})] \\ &\quad + U_t \cos\phi \sin\delta [U_{i2}^{\infty}(\mathbf{x}) + U_{i2}^{\mathrm{c}}(\mathbf{x})] \\ &\quad - U_t \cos\delta [U_{i3}^{\infty}(\mathbf{x}) + U_{i3}^{\mathrm{c}}(\mathbf{x})], \\ \frac{\partial u_i(\mathbf{x})}{\partial x_j} &= -U_t \sin\phi \sin\delta \left[\frac{\partial U_{i1}^{\infty}(\mathbf{x})}{\partial x_j} + \frac{\partial U_{i1}^{\mathrm{c}}(\mathbf{x})}{\partial x_j} \right] \\ &\quad + U_t \cos\phi \sin\delta \left[\frac{\partial U_{i2}^{\infty}(\mathbf{x})}{\partial x_j} + \frac{\partial U_{i2}^{\mathrm{c}}(\mathbf{x})}{\partial x_j} \right] \\ &\quad - U_t \cos\delta \left[\frac{\partial U_{i3}^{\infty}(\mathbf{x})}{\partial x_j} + \frac{\partial U_{i3}^{\mathrm{c}}(\mathbf{x})}{\partial x_j} \right]. \end{aligned} \tag{35c}$$

Because the polygonal dislocation is composed of a finite number of end-to-end straight segments, the elastic fields of a polygonal dislocation can be found by simply superposing all the solutions corresponding to the straight segments of the polygon. For a directional straight segment AB, beginning at point $\mathbf{x}^A$ and ending at point $\mathbf{x}^B$, the induced displacements $u_i(\mathbf{x})$ and their derivatives (or distortions) $\partial u_i(\mathbf{x})/\partial x_j$ are still given by equation (35), with $U_{ij}^{\infty}(\mathbf{x})$, $U_{ij}^{\mathrm{c}}(\mathbf{x})$, $\partial U_{ij}^{\infty}(\mathbf{x})/\partial x_k$, and $\partial U_{ij}^{\mathrm{c}}(\mathbf{x})/\partial x_k$ also defined in equations (23), (24), (30), and (31), respectively. In equations (23), (24), (30), and (31), however, the line integrals over the straight segment AB can be expressed analytically in terms of elementary functions as listed in detail in Appendix A and coded in Ⓔ MATLAB (four MATLAB codes are available in the electronic supplement: one for a rectangular dislocation, one for a triangular dislocation, and the other two for comparison of displacements between the present and Okada codes).

Numerical Examples

Before applying our solutions to a general polygonal dislocation embedded in a transversely isotropic half-space, we should point out that by taking the proper limits, our analytical solutions will reduce to those in Okada (1992). Furthermore, as we mentioned earlier and will show below, our formulations can be directly compared with the Okada (1992) problem of a rectangular dislocation in an isotropic half-space. A rectangular dislocation having a dimension of 12 km × 8 km with $\phi = 0°$ and $\delta = 40°$ and its lower edge located 10 km below the free surface is shown in Figure 2. Results are shown for three different displacement discontinuity cases (i.e., $U_{\mathrm{s}} = 50$ cm, or $U_{\mathrm{d}} = 50$ cm, or $U_{\mathrm{t}} = 50$ cm), representing an earthquake source of approximately M_{w} 6. We assume that $\lambda = \mu$, in which λ and μ are the two Lamé constants of the isotropic material. To directly use our transversely isotropic formulations for the isotropic case, the five elastic constants are selected to be close to the isotropic case by, for instance, letting $c_{44} = \mu(1 + 0.00001)$, $c_{66} = \mu(1 + 0.00003)$, $c_{13} = \lambda(1 + 0.00005)$, $c_{11} = (\lambda + 2\mu)(1 + 0.00007)$, and $c_{33} = (\lambda + 2\mu)(1 + 0.00009)$. If the

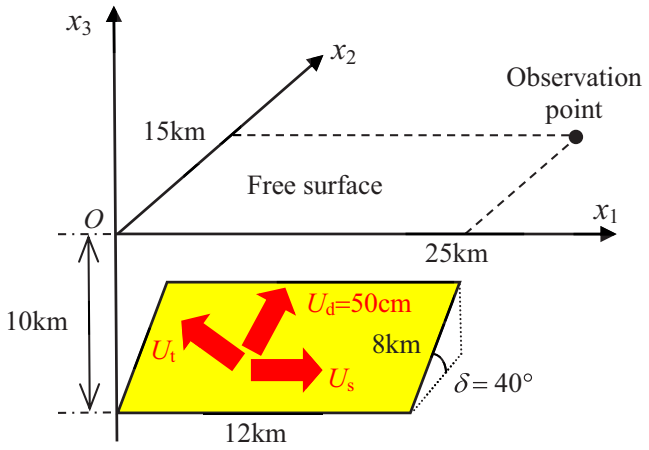

Figure 2. A rectangular dislocation of dimension 12 km × 8 km with $U_s = 50$ cm (or $U_d = 50$ cm, or $U_t = 50$ cm) in an isotropic half-space. The lower edge of the rectangle is 10 km below the surface. The strike direction of the fault is parallel to the x_1 axis and the dip angle is $\delta = 40°$. The field points are along the depth direction with fixed horizontal coordinates $(x_1, x_2) = (25, 15)$ km. The color version of this figure is available only in the electronic edition.

second proportional factors in these constants (c_{ij}) all equal 1, the material becomes isotropic. Therefore, an arbitrary small value (e.g., 10^{-5}–10^{-6}) is added to make the proportional factors slightly different from 1 but very close to the isotropic case so that the solutions presented in this article can still be directly compared with the isotropic case (Pan, 1997). The strains (referring generally to strains, tilts, and deformation gradients) beneath the observation point $(x_1, x_2) = (25, 15)$ km along a vertical observation line ranging from 0 to 20 km depth are evaluated for the strike-slip fault with $U_s = 50$ cm, the dip-slip fault with $U_d = 50$ cm, and the tensile fracture with $U_t = 50$ cm, respectively. One can observe from Figure 3 that our results are exactly the same as those in Okada (1992), which verifies that our formulations for the transversely isotropic rocks are correct in this limit and that they can be further directly compared with the isotropic half-space case. Comparison of displacements between our solution and the solution by Okada (1992) for the same problem, as described in Figure 2, is provided in the Ⓔ electronic supplement, along with the corresponding MATLAB codes.

A Rectangular Dislocation in a Transversely Isotropic Half-Space

As the first numerical example, we investigate the effect of rock anisotropy on strains due to rectangular dislocations (or faults). Rock anisotropy has been well documented, and the source of anisotropy may be intrinsic (due to bedding or laminations in sedimentary rocks or aligned minerals forming foliations in metamorphic rocks) or extrinsic (formed by stress-induced cracking of intrinsically isotropic rocks). In this article, two representative examples of intrinsic, trans-

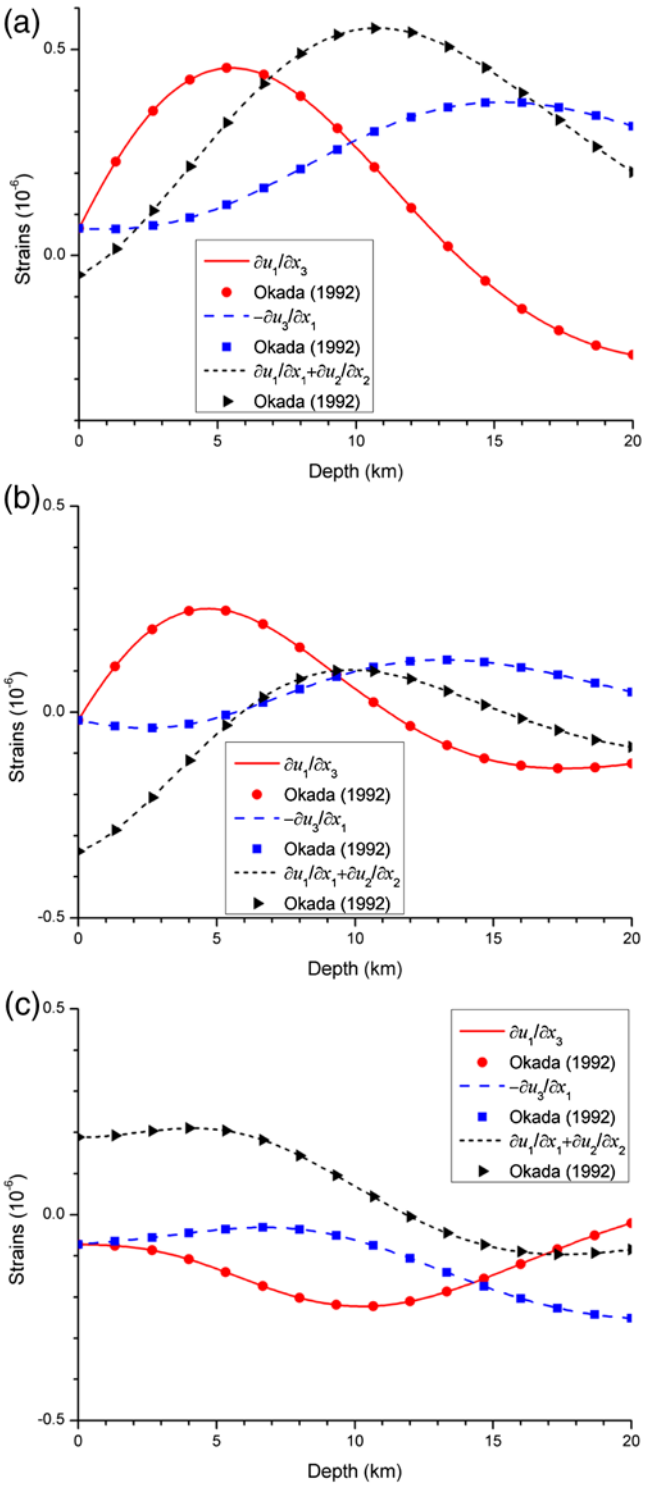

Figure 3. Variation of strains (general names for strains, tilts, and deformation gradients) beneath the observation point $(x_1, x_2) = (25, 15)$ km for (a) strike-slip fault with $U_s = 50$ cm, (b) dip-slip fault with $U_d = 50$ cm, and (c) tensile fracture with $U_t = 50$ cm in an isotropic half-space. The geometry of the rectangular dislocation is shown in Figure 2. The color version of this figure is available only in the electronic edition.

Table 1
Elastic Coefficients (c_{ij}) of Two Typical Transversely Isotropic Rock Materials and Their Voigt Averages (λ and μ) in GPa

	c_{11}	c_{33}	c_{44}	c_{66}	c_{13}
Material 1	113	87	30	41.5	22
Voigt average of material 1		$\lambda = 27.1$, $\mu = 36.2$			
Material 2	25	19	5	7	10
Voigt average of material 2		$\lambda = 10.6$, $\mu = 5.9$			

versely isotropic rock are selected, with one being strongly anisotropic and the other only weakly anisotropic. Both representative datasets are obtained from measurements of rock velocities in multiple directions with respect to the dominant rock fabric. The first set with strong anisotropy is the average of the rock properties in the garnet-oligoclase zone of the Haast schist, a prominent metamorphic belt south of the Alpine fault in New Zealand, where foliation is approximately vertical (Godfrey *et al.*, 2000). The second set with weak anisotropy is the average of the rock properties in North Sea shale, with ~20% *P*-wave anisotropy (Wang, 2002). In the numerical calculations, we assume the dislocation model is exactly the same as in Figure 2 (but with transverse isotropy) and that the plane of isotropy of the material is parallel to the free surface of the half-space (i.e., the x_1–x_2 plane). The five independent stiffness constants are listed in Table 1. For comparison, their corresponding Voigt averages are also used to calculate the induced strains in the equivalent isotropic rock half-space. The Voigt average assumes $(c_{ijij})^{\text{aniso.}} = (c_{ijij})^{\text{iso.}}$ and $(c_{iijj})^{\text{aniso.}} = (c_{iijj})^{\text{iso.}}$. For transversely isotropic materials, the Voigt average is defined as $\lambda = (c_{11} + c_{33} + 5c_{12} + 8c_{13} - 4c_{44})/15$ and $\mu = (7c_{11} - 5c_{12} + 2c_{33} + 12c_{44} - 4c_{13})/30$, in which λ and μ are the equivalent Lamé constants (Hirth and Lothe, 1982). Again, the isotropic material property is slightly perturbed (as described above) so that we can directly make use of our solutions for transverse isotropy.

Once again, the strains beneath the observation point $(x_1, x_2) = (25, 15)$ km with depth ranging from 0 to 20 km are evaluated for the strike-slip fault with $U_s = 50$ cm, the dip-slip fault with $U_d = 50$ cm, and the tensile fracture with $U_t = 50$ cm, respectively, and for materials 1 (strongly anisotropic) and 2 (weakly anisotropic) and their isotropic equivalents. For this case, although all the strains are influenced by the rock anisotropy, the strain component $\partial u_1/\partial x_3$ is strikingly affected, as compared to the isotropic one (Figs. 4 and 5). The relative difference between the transversely isotropic and isotropic solutions for this component can be over 200% for material 1 with strong anisotropy and over 100% for material 2 with weak anisotropy. Thus, the elastic anisotropy of rocks should be considered to accurately predict the static field of dislocations in transversely isotropic rocks.

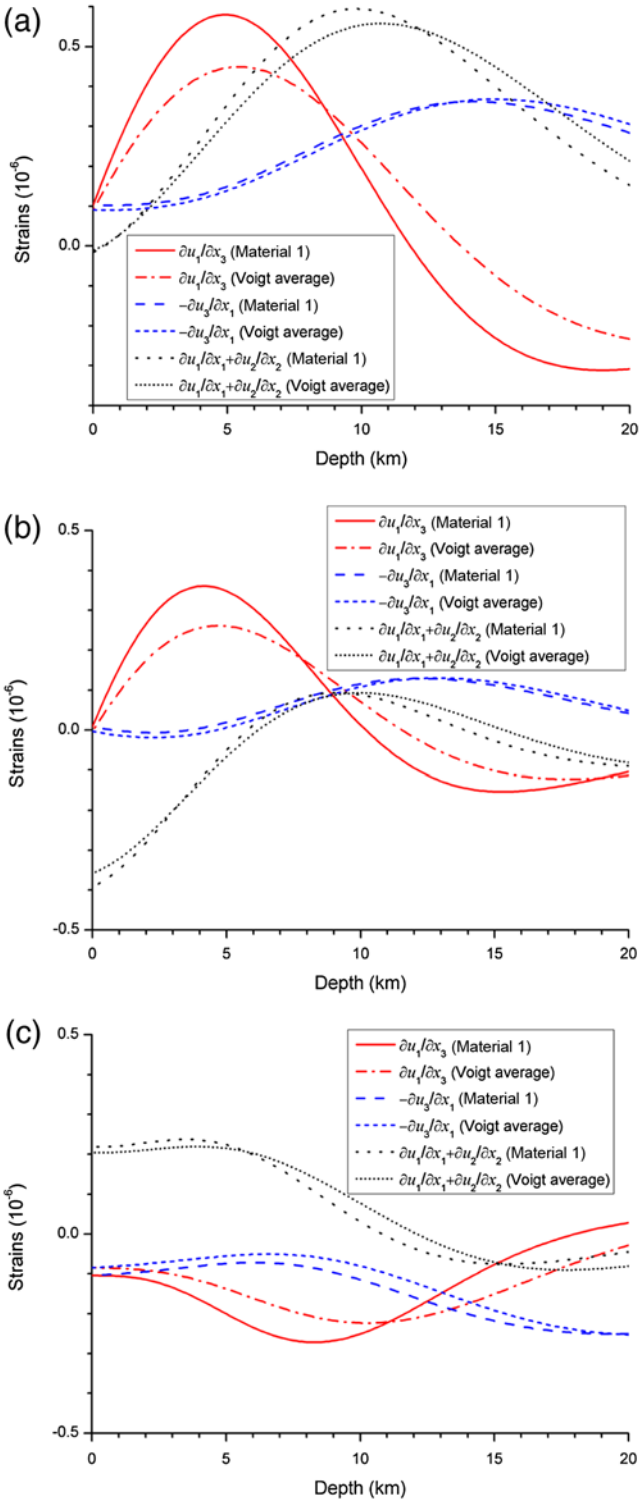

Figure 4. Variation of strains beneath the observation point $(x_1, x_2) = (25, 15)$ km for (a) strike-slip fault with $U_s = 50$ cm, (b) dip-slip fault with $U_d = 50$ cm, and (c) tensile fracture with $U_t = 50$ cm in a half-space occupied by the transversely isotropic material 1 (or an isotropic material equivalent to material 1 by Voigt average). The geometry of the rectangular dislocation is the same as in Figure 2. The color version of this figure is available only in the electronic edition.

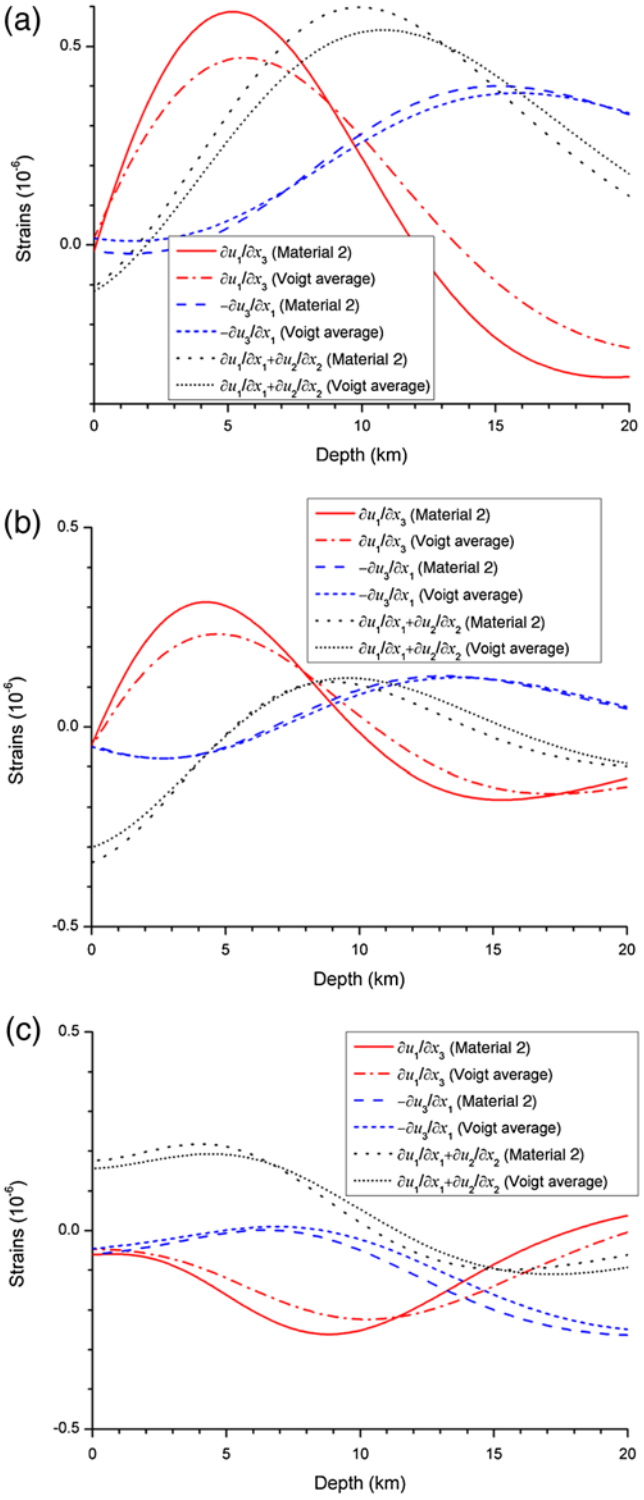

Figure 5. Variation of strains beneath the observation point $(x_1, x_2) = (25, 15)$ km for (a) strike-slip fault with $U_s = 50$ cm, (b) dip-slip fault with $U_d = 50$ cm, and (c) tensile fracture with $U_t = 50$ cm in a half-space occupied by the transversely isotropic material 2 (or an isotropic material equivalent to material 2 by Voigt average). The geometry of the rectangular dislocation is the same as in Figure 2. The color version of this figure is available only in the electronic edition.

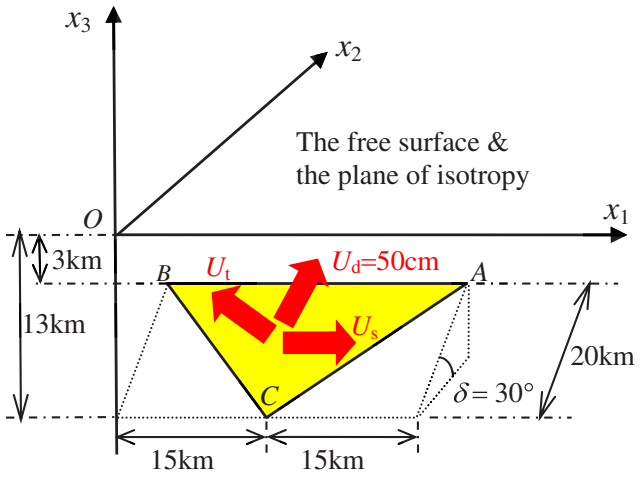

Figure 6. A triangular dislocation with $U_s = 50$ cm (or $U_d = 50$ cm, or $U_t = 50$ cm) in a transversely isotropic half-space. The upper side AB of the triangle is parallel to the x_1 axis and it is 3 km below the free surface. The side BC and CA are of the same length. The strike direction of the fault is parallel to the x_1 axis and the dip angle is $\delta = 30°$. The color version of this figure is available only in the electronic edition.

A Triangular Dislocation in a Transversely Isotropic Half-Space

As the second example, we consider a buried triangular dislocation in the half-space occupied by transversely isotropic material 1 (see Table 1). It is well known that both the Northridge and Puente Hills thrust faults of the Los Angeles basins attributed to $M_w > 5.9$ earthquakes in the last three decades (e.g., Yeats and Huftile, 1995; Shaw and Shearer, 1999). Both faults are blind in the sense that their upper tip lines are below the surface of the Earth. For thrust faults, representative of those ruptured in the Los Angeles basin as discussed above, we use a representative fault size of about 30 km × 20 km and dip angle of about 30°. We thus investigate a representative triangular dislocation ABC with the following three vertices: $A(30, 10\sqrt{3}, -3)$ km, $B(0, 10\sqrt{3}, -3)$ km, and $C(15, 0, -13)$ km, as shown in Figure 6. In the following calculations, the displacement discontinuity over the fault plane is assumed to be $U_s = 50$ cm (or $U_d = 50$ cm, or $U_t = 50$ cm, separately). We also assume the plane of isotropy of material 1 is parallel to the free surface of the half-space (i.e., the x_1–x_2 plane). Numerical results are shown in Figures 7 and 8 for the transversely isotropic material 1 and are compared with the results based on the isotropic Voigt average.

Figure 7 shows the strains beneath the observation point $(x_1, x_2) = (45, -15)$ km with depth ranging from 0 to 25 km for the strike-slip fault with $U_s = 50$ cm (Fig. 7a), the dip-slip fault with $U_d = 50$ cm (Fig. 7b), and the tensile fracture with $U_t = 50$ cm (Fig. 7c), respectively. The strain $\partial u_1/\partial x_3$ is much more sensitive to material anisotropy than the tilt $\partial u_3/\partial x_1$ and the areal dilatation $\partial u_1/\partial x_1 + \partial u_2/\partial x_2$, regardless of the fault model (Fig. 7).

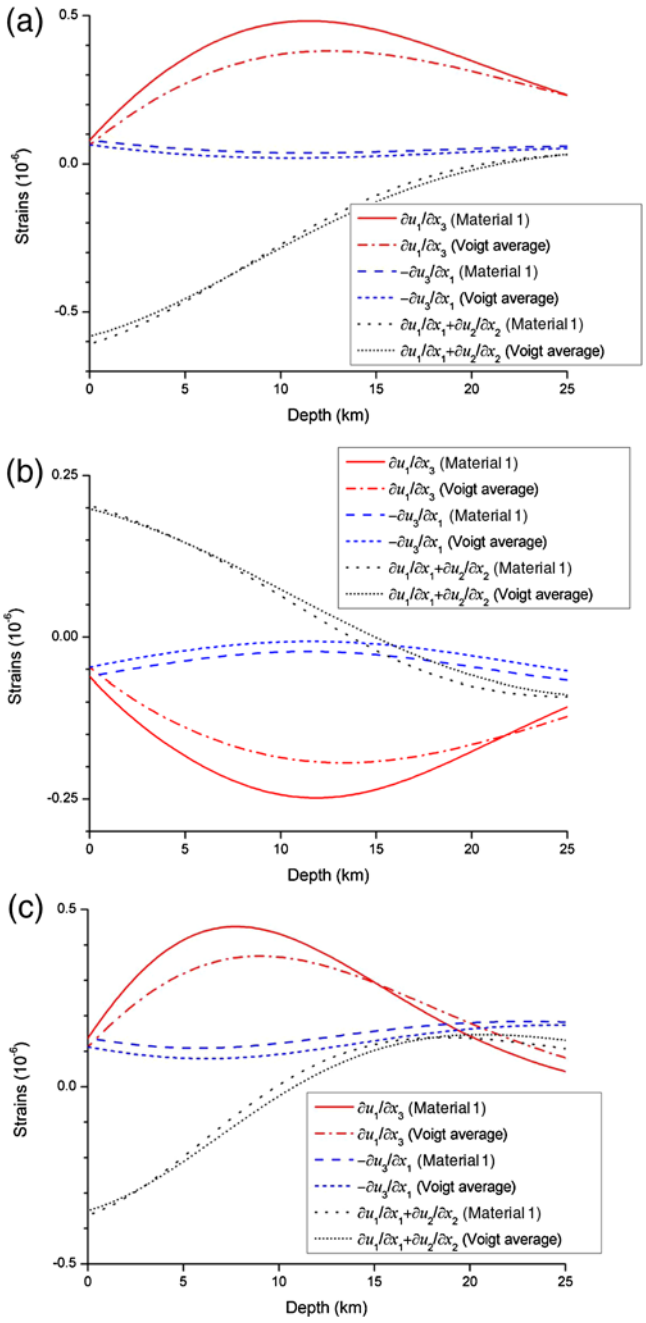

Figure 7. Variation of strains beneath the observation point $(x_1, x_2) = (45, -15)$ km for (a) strike-slip fault with $U_s = 50$ cm, (b) dip-slip fault with $U_d = 50$ cm, and (c) tensile fracture with $U_t = 50$ cm in a half-space occupied by transversely isotropic material 1 (or an isotropic material equivalent to material 1 by Voigt average). The geometry of the triangular dislocation is shown in Figure 6. The color version of this figure is available only in the electronic edition.

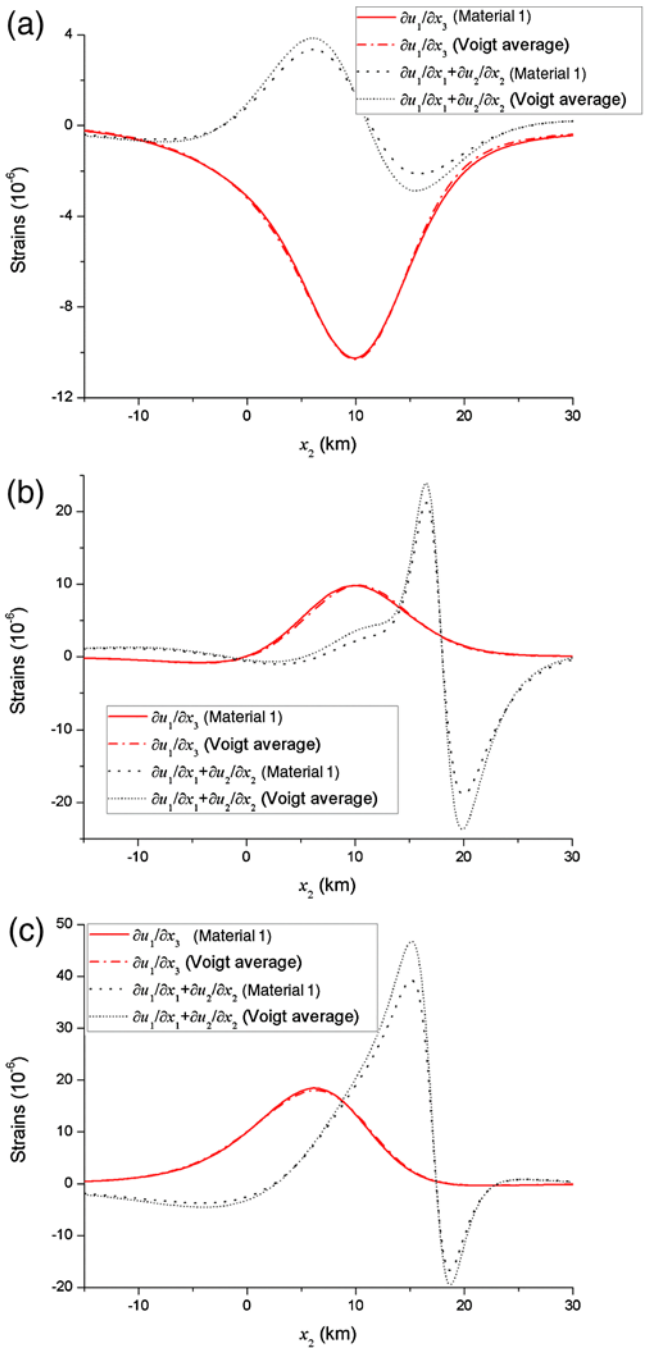

Figure 8. Surface strains as functions of x_2 (with fixed $(x_1, x_3) = (20, 0)$ km) for (a) strike-slip fault with $U_s = 50$ cm, (b) dip-slip fault with $U_d = 50$ cm, and (c) tensile fracture with $U_t = 50$ cm in a half-space occupied by the transversely isotropic material 1 and by an isotropic material equivalent to material 1 by Voigt average, as listed in Table 1. The geometry of the triangular dislocation is shown in Figure 6. The color version of this figure is available only in the electronic edition.

Figure 8 shows the variation of surface strains ($x_3 = 0$) with the location of the observation point for the strike-slip fault with $U_s = 50$ cm (Fig. 8a), the dip-slip fault with $U_d = 50$ cm (Fig. 8b), and the tensile fracture with $U_t = 50$ cm (Fig. 8c), respectively, in which x_1 is fixed at 20 km and x_2 ranges from -15 to 30 km. Along this line, the material anisotropy has a considerable effect on both the surface strain $(\partial u_1/\partial x_3)$ and the surface area-dilatation $(\partial u_1/\partial x_1 + \partial u_2/\partial x_2)$, with the maximum differences of over 40% between the isotropic and anisotropic models.

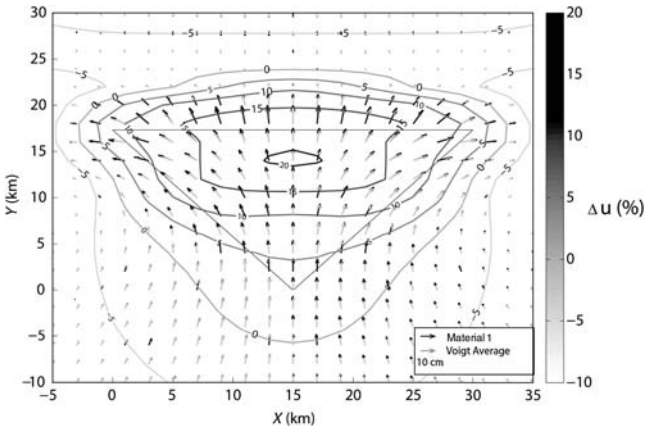

Figure 9. Horizontal displacement vector fields on the surface due to the triangular fault with $U_d = 50$ cm in Figure 6. Black arrows correspond to displacements in transversely isotropic material 1 and gray arrows to those in the Voigt average isotropic material 1 (Table 1). Contours of Δu are the percentage difference in magnitude between material 1 and its Voigt average material, as defined in equation (36).

To examine the spatial differences of surface displacements, we plot the horizontal displacement vector (u_1, u_2) in terms of its magnitude $u = \sqrt{u_1^2 + u_2^2}$ and orientation in the x_1–x_2 plane as shown in Figure 9. The fault is of triangular shape with $U_d = 50$ cm (Fig. 6), and both material 1 and its Voigt average are considered (Table 1). Although the surface displacement fields are similar for both material 1 and its Voigt average, the discrepancies in magnitude and direction of the displacements are heterogeneously distributed throughout the surface domain over the fault (Fig. 9). For example, the difference in the surface displacement magnitude Δu between material 1 and its Voigt average, defined as

$$\Delta u = \frac{u_{\text{Voigt}} - u_{\text{material 1}}}{u_{\text{Voigt}}}, \tag{36}$$

can be over 20% and the discrepancy in the orientation can be as large as $\pm 4°$.

Conclusions

Based on the concepts of the dislocation loop and dislocation segment, we derived a complete set of analytical solutions for displacements and strains due to a dislocation of general polygonal shape in a three-dimensional transversely isotropic half-space. Our solutions reproduce the well-known results of Okada (1992) for a rectangular dislocation in an isotropic half-space as a special case. We also point out that our solutions are applicable to both blind faults and faults that intersect the free surface. Because our solutions are in exact closed forms for any polygonal dislocation, one can simply superpose these solutions to find the elastic fields of an arbitrary dislocation. Our numerical examples reveal the important effect of material anisotropy on the internal and surface strains and surface deformations due to polygonal dislocations. Our solutions should be particularly appealing for researchers who are interested in the static displacement or strain fields due to a dislocation of arbitrary shape with nonuniform Burgers vector in transversely isotropic rock half-spaces.

Data and Resources

All data used in this article came from published sources listed in the references. The second numerical example was based on the approximate geometry and size of the Northridge fault as defined in the Southern California Earthquake Center community fault model at http://structure.rc.fas.harvard.edu/cfm/modelaccess.html (last accessed March 2013).

Acknowledgments

The first author (E. P.) has benefitted a lot from his discussions with Mike Bevis of Ohio State University since 2006 on triangular dislocations and related issues. The authors would like to thank many people for their constructive comments on the earlier versions of the paper and the corresponding MATLAB codes. Particular thanks go to Y. Okada and K. X. Hao of National Research Institute for Earth Science and Disaster Prevention for their encouragement and comments on the paper and the corresponding codes. We also would like to thank the Associate Editor Roland Bürgmann and the two anonymous reviewers for their useful comments on the manuscript. This work is supported by the National Project of Scientific and Technical Supporting Programs funded by Ministry of Science and Technology of China (Number 2009BAG12A01-A03-2). It is also partially supported by the National Natural Science Foundation of China (Numbers 10972196, 11321202, and 11172273) and by the United States National Institute for Occupational Health and Safety Award Number 1R03OH010112-01A1.

References

Amadei, B. (1996). Importance of anisotropy when estimating and measuring in situ stresses in rock, *Int. J. Rock Mech. Min. Sci. Geomech. Abstr.* **33,** 293–325.

Amelung, F., S. Yun, T. R. Walter, P. Segall, and S. Kim (2007). Stress control of deep rift intrusion at Mauna Loa volcano, Hawaii, *Science* **316,** 1026–1030, doi: 10.1126/science.1140035.

Chan, A. W., and M. D. Zoback (2007). The role of hydrocarbon production on land subsidence and fault reactivation in the Louisiana coastal zone, *J. Coastal Res.* **23,** 771–786.

Comninou, M. A., and J. Dunders (1975). The angular dislocation in a half-space, *J. Elasticity* **5,** 203–216.

Delaney, P. T., and D. D. Pollard (1981). Deformation of host rocks and flow of magma during growth of minette dikes and breccia-bearing intrusions near Ship Rock, New Mexico, *Geol. Soc. Profess. Pap. 1202*.

Ding, H. J., W. Q. Chen, and L. C. Zhang (2006). *Elasticity of Transversely Isotropic Materials*, Springer, Dordrecht, The Netherlands.

Fabrikant, V. I. (2004). A new form of the Green function for a transversely isotropic body, *Acta Mech.* **167,** 101–111.

Freund, L. B., and D. M. Barnett (1976). A two-dimensional analysis of surface deformation due to dip-slip faulting, *Bull. Seismol. Soc. Am.* **66,** 667–675.

Gercek, H. (2007). Poisson's ratio values for rocks, *Int. J. Rock Mech. Min. Sci. Geomech. Abstr.* **44,** 1–13.

Godfrey, N. J., N. I. Christensen, and D. A. Okaya (2000). Anisotropy of schists: Contribution of crustal anisotropy to active source seismic experiments and shear wave splitting observations, *J. Geophys. Res.* **105,** 27,991–28,007.

Griffith, W. A., and M. L. Cooke (2004). Mechanical validation of the three-dimensional intersection geometry between the Puente Hills blind-thrust system and the Whittier fault, Los Angeles, California, *Bull. Seismol. Soc. Am.* **94,** 493–505.

Hirth, J. P., and J. Lothe (1982). *Theory of Dislocations*, Second Ed., John Wiley & Sons, New York, New York.

Jeyakumaran, M., J. W. Rudnicki, and L. M. Keer (1992). Modeling slip zones with triangular dislocation elements, *Bull. Seismol. Soc. Am.* **82,** 2153–2169.

Johnsson, S., H. Zebker, P. Segall, and F. Amelung (2002). Fault slip distribution of the 1999 M_w 7.1 Hector Mine, California, earthquake, estimated from satellite radar and GPS measurements, *Bull. Seismol. Soc. Am.* **92,** 1377–1389.

King, G. C. P., R. S. Stein, and J. Lin (1994). Static stress changes and the triggering of earthquakes, *Bull. Seismol. Soc. Am.* **84,** 935–953.

Maerten, F., L. Maerten, and D. D. Pollard (2014). iBem3D, a three-dimensional iterative boundary element method using angular dislocations for modeling geologic structures, *Comput. Geosci.* **72,** 1–17, doi: 10.1016/j.cageo.2014.06.007.

Maerten, F., P. Resor, D. D. Pollard, and L. Maerten (2005). Inverting for slip on three-dimensional fault surfaces using angular dislocations, *Bull. Seismol. Soc. Am.* **95,** 1654–1665.

Maerten, L., P. Gillespie, and D. D. Pollard (2002). Effect of local stress perturbation on secondary fault development, *J. Struct. Geol.* **24,** 145–153.

Meade, B. J. (2007). Algorithms for the calculation of exact displacements, strains, and stresses for triangular dislocation elements in a uniform elastic half space, *Comput. Geosci.* **33,** 1064–1075.

Micklethwaite, S., and S. F. Cox (2004). Fault-segment rupture, aftershock-zone fluid flow, and mineralization, *Geology* **32,** 813–816, doi: 10.1130/G20559.1.

Muller, J. R., A. Aydin, and T. J. Wright (2006). Using an elastic dislocation model to investigate static Coulomb stress change scenarios for earthquake ruptures in the eastern Marmara Sea region, Turkey, in *Analogue and Numerical Modelling of Crustal-Scale Processes*, S. J. H. Buiter and G. Schreurs (Editors), Special Publication, Vol. 253, Geological Society, London, United Kingdom, 397–414.

Okada, Y. (1985). Surface deformation due to shear and tensile faults in a half-space, *Bull. Seismol. Soc. Am.* **75,** 1135–1154.

Okada, Y. (1992). Internal deformation due to shear and tensile faults in a half-space, *Bull. Seismol. Soc. Am.* **82,** 1018–1040.

Pan, E. (1989). Static response of a transversely isotropic and layered half-space to general dislocation sources, *Phys. Earth Planet. In.* **58,** 103–117.

Pan, E. (1991). Dislocation in an infinite poroelastic medium, *Acta Mech.* **87,** 105–115.

Pan, E. (1997). A general boundary element analysis of 2-D linear elastic fracture mechanics, *Int. J. Fract.* **88,** 41–59.

Pan, Y. C., and T. W. Chou (1976). Point force solution for an infinite transversely isotropic solid, *ASME J. Appl. Mech.* **43,** no. 4, 608–612.

Segall, P. (2007). *Earthquake and Volcano Deformation*, Princeton University Press, Princeton, New Jersey, 432 pp.

Shaw, J. H., and P. M. Shearer (1999). An elusive blind-thrust fault beneath metropolitan Los Angeles, *Science* **283,** 1516–1518.

Thatcher, W. (1975). Strain accumulation and release mechanism of the 1906 San Francisco earthquake, *J. Geophys. Res.* **80,** 4862–4872.

Thomas, A. L. (1993). Poly3D: A three-dimensional, polygonal element, displacement discontinuity boundary element computer program with applications to fractures, faults, and cavities in the Earth's crust, *M.S. Thesis*, Stanford University, Stanford, California, 68 pp.

Wang, C. D., and J. J. Liao (1998). Stress influence charts for transversely isotropic rocks, *Int. J. Rock Mech. Min. Sci. Geomech. Abstr.* **35,** 771–785.

Wang, Z. (2002). Seismic anisotropy in sedimentary rocks, part 2: Laboratory data, *Geophysics* **67,** 1423–1440.

Yeats, R. S., and G. J. Huftile (1995). The Oak Ridge fault system and the 1994 Northridge earthquake, *Nature* **373,** 418–420.

Yoffe, E. H. (1960). The angular dislocation, *Phil. Mag.* **5,** 161–175.

Yoffe, E. H. (1961). A dislocation at a free surface, *Phil. Mag.* **6,** 1147–1155.

Yuan, J. H., W. Q. Chen, and E. Pan (2013). Line-integral representations of the displacement and stress fields due to an arbitrary Volterra dislocation loop in a transversely isotropic elastic full-space, *Int. J. Solids Struct.* **50,** 160–175.

Yuan, J. H., E. Pan, and W. Q. Chen (2013). Line-integral representations for the elastic displacements, stresses and interaction energy of arbitrary dislocation loops in transversely isotropic bimaterials, *Int. J. Solids Struct.* **50,** 3472–3489.

Yun, S., P. Segall, and H. Zebker (2006). Constraints on magma chamber geometry at Sierra Negra Volcano, Galapogos Islands, based on InSAR observations, *J. Volcanol. Geoth. Res.* **150,** 232–243.

Appendix A

Analytical Integration of the Displacement and Distortion Fields due to a Straight Segment AB of the Dislocation Loop

The line integrals involved in equations (23a–e), (24a–e), (30a–h), and (31a–h) for the displacement and distortion fields of the dislocation loop can be carried out exactly over the straight segment AB in terms of elementary functions. We now list the analytical results below.

$$4\pi(-1)^{\xi}U^{\infty}_{\xi\xi}(\mathbf{x}) = -(-1)^{\xi}\Omega^{\infty}_{3} - g_i s_i \mathrm{I22}(\,) - 2s_3^2 f_i \gamma_i \mathrm{Cj2}(\,)$$
$$\Omega^{\infty}_{3}(\mathbf{x}) = -\mathrm{sgn}\langle S(x_1,x_2) - x_3\rangle \mathrm{Cbar}(\,) - s_3 \mathrm{CjN}(\,), \tag{A1a}$$

$$4\pi(-1)^{\xi}U^{\infty}_{\xi(3-\xi)}(\mathbf{x}) = s_3 \mathrm{I00}(\,) + g_i s_i \mathrm{I22}(\,) - 2s_3^2 f_i \gamma_i \mathrm{Cj}(\,) + 2s_3^2 f_i \gamma_i \mathrm{Cj2}(\,), \tag{A1b}$$

$$4\pi(-1)^{\xi}U^{\infty}_{3(3-\xi)}(\mathbf{x}) = -m_\beta s_\beta [2s_3^2 f_\beta \mathrm{I22}(\,) + g_\beta \mathrm{I00}(\,)], \tag{A1c}$$

$$4\pi(-1)^{\xi}U^{\infty}_{(3-\xi)3}(\mathbf{x}) = -g_i s_i \mathrm{I22}(\,) - g_\alpha \gamma_\alpha \mathrm{I00}(\,), \tag{A1d}$$

$$4\pi U^{\infty}_{33}(\mathbf{x}) = \mathrm{sgn}\langle S(x_1,x_2) - x_3\rangle \mathrm{Cbar}(\,) + m_\beta g_\beta s_\beta \mathrm{CjN}(\,); \tag{A1e}$$

$$4\pi(-1)^{\xi}U^{c}_{\xi\xi}(\mathbf{x}) = (-1)^{\xi}[-\mathrm{Cbar}(\,) + s_3 \mathrm{CjN}(\,)] - g_{ij} s_i \mathrm{I22}(\,)$$
$$- 2s_3^2 f_{ij} \gamma_i \mathrm{Cj2}(\,) - 4s_3^2 f_{ij} \mathrm{L43}(\,), \tag{A2a}$$

$$4\pi(-1)^{\xi}U^{c}_{\xi(3-\xi)}(\mathbf{x}) = s_3\mathrm{I00}() + g_{ij}s_i\mathrm{I22}() - 2s_3^2 f_{ij}\gamma_i\mathrm{Cj}() + 2s_3^2 f_{ij}\gamma_i\mathrm{Cj2}() + 2s_3^2 f_{ij}\mathrm{Cbar1}(), \tag{A2b}$$

$$4\pi(-1)^{\xi}U^{c}_{3(3-\xi)}(\mathbf{x}) = m_\beta s_\beta[2s_3^2 f_{\alpha\beta}\mathrm{I22}() + g_{\alpha\beta}\mathrm{I00}()] + 2s_3^2 F\mathrm{L21}(), \tag{A2c}$$

$$4\pi(-1)^{\xi}U^{c}_{(3-\xi)3}(\mathbf{x}) = -g_{ij}s_i\mathrm{I22}() - g_{\alpha\beta}\gamma_\alpha\mathrm{I00}(), \tag{A2d}$$

$$4\pi U^{c}_{33}(\mathbf{x}) = -\mathrm{Cbar}() - m_\beta g_{\alpha\beta}s_\beta\mathrm{CjN}(); \tag{A2e}$$

$$4\pi(-1)^{\xi}\frac{\partial U^{\infty}_{\eta(3-\xi)}(\mathbf{x})}{\partial x_\tau} = \varepsilon_{\eta\xi 3}(-1)^{\tau}s_3[\mathrm{J01}(3;3-\tau) - \mathrm{J01}(3-\tau;3)] + \delta_{\eta\xi}s_3\mathrm{J01}(\tau;3) + g_i s_i\mathrm{Cjk2}() + 2s_3^2 f_i\gamma_i\mathrm{Cj3}(), \tag{A3a}$$

$$4\pi(-1)^{\xi}\frac{\partial U^{\infty}_{\eta(3-\xi)}(\mathbf{x})}{\partial x_3} = \delta_{\eta\xi}s_3^3\mathrm{J01}(3;3) - s_3\mathrm{J01}(\xi;\eta) - g_\beta s_\beta\mathrm{J01}(\eta;\xi) - 2s_3^2 f_j s_j\mathrm{Cjk2}(), \tag{A3b}$$

$$4\pi(-1)^{\xi}\frac{\partial U^{\infty}_{3(3-\xi)}(\mathbf{x})}{\partial x_\tau} = -m_\beta g_\beta s_\beta\mathrm{J01}(\tau;\xi) - 2s_3^2 m_\beta f_\beta s_\beta\mathrm{Cjk2}(), \tag{A3c}$$

$$4\pi(-1)^{\xi}\frac{\partial U^{\infty}_{3(3-\xi)}(\mathbf{x})}{\partial x_3} = -m_\beta s_\beta^2[g_\beta s_\beta\mathrm{J01}(3;\xi) - 2s_3^2 f_\beta\gamma_\beta\mathrm{J01}(\xi;3)], \tag{A3d}$$

$$4\pi(-1)^{\xi}\frac{\partial U^{\infty}_{(3-\xi)3}(\mathbf{x})}{\partial x_\tau} = -g_\beta\gamma_\beta\mathrm{J01}(\tau;\xi) - g_i s_i\mathrm{Cjk2}(), \tag{A3e}$$

$$4\pi(-1)^{\xi}\frac{\partial U^{\infty}_{(3-\xi)3}(\mathbf{x})}{\partial x_3} = -g_\beta s_\beta\mathrm{J01}(3;\xi) + g_i s_i\mathrm{J01}(\xi;3), \tag{A3f}$$

$$4\pi\frac{\partial U^{\infty}_{33}(\mathbf{x})}{\partial x_\tau} = -(-1)^{\tau}m_\beta g_\beta s_\beta[\mathrm{J01}(3-\tau;3) - \mathrm{J01}(3;3-\tau)], \tag{A3g}$$

$$4\pi\frac{\partial U^{\infty}_{33}(\mathbf{x})}{\partial x_3} = m_\beta g_\beta s_\beta[\mathrm{J01}(1;2) - \mathrm{J01}(2;1)]; \tag{A3h}$$

$$4\pi(-1)^{\xi}\frac{\partial U^{c}_{\eta(3-\xi)}(\mathbf{x})}{\partial x_\tau} = \varepsilon_{\eta\xi 3}(-1)^{\tau}s_3[\mathrm{J01}(3;3-\tau) - \mathrm{J01}(3-\tau;3)] + \delta_{\eta\xi}s_3\mathrm{J01}(\tau;3) + g_{ij}s_i\mathrm{Cjk2}() + 2s_3^2 f_{ij}\gamma_i[\mathrm{Cj3}() + 2s_i\mathrm{Cbar3}()], \tag{A4a}$$

$$4\pi(-1)^{\xi}\frac{\partial U^{c}_{\eta(3-\xi)}(\mathbf{x})}{\partial x_3} = -\delta_{\eta\xi}s_3^3\mathrm{J01}(3;3) + s_3\mathrm{J01}(\xi;\eta) + g_{\alpha\beta}s_\beta\mathrm{J01}(\eta;\xi) + 2s_3^2[f_{ij}s_j\mathrm{Cjk2}() - F\mathrm{Cbar2}()], \tag{A4b}$$

$$4\pi(-1)^{\xi}\frac{\partial U^{c}_{3(3-\xi)}(\mathbf{x})}{\partial x_\tau} = m_\beta g_{\alpha\beta}s_\beta\mathrm{J01}(\tau;\xi) + 2s_3^2[m_\beta f_{\alpha\beta}s_\beta\mathrm{Cjk2}() + F\mathrm{Cbar2}()], \tag{A4c}$$

$$4\pi(-1)^{\xi}\frac{\partial U^{c}_{3(3-\xi)}(\mathbf{x})}{\partial x_3} = -m_\beta s_\beta^2[g_{\alpha\beta}s_\alpha\mathrm{J01}(3;\xi) - 2s_3^2 f_{\alpha\beta}\gamma_\alpha\mathrm{J01}(\xi;3)], \tag{A4d}$$

$$4\pi(-1)^{\xi}\frac{\partial U^{c}_{(3-\xi)3}(\mathbf{x})}{\partial x_\tau} = -g_{\alpha\beta}\gamma_\alpha\mathrm{J01}(\tau;\xi) - g_{ij}s_i\mathrm{Cjk2}(), \tag{A4e}$$

$$4\pi(-1)^{\xi}\frac{\partial U^{c}_{(3-\xi)3}(\mathbf{x})}{\partial x_3} = g_{\alpha\beta}s_{\beta}\mathrm{J01}(3;\xi) - g_{ij}s_{j}\mathrm{J01}(\xi;3), \tag{A4f}$$

$$4\pi\frac{\partial U^{c}_{33}(\mathbf{x})}{\partial x_{\tau}} = (-1)^{\tau}m_{\beta}g_{\alpha\beta}s_{\beta}[\mathrm{J01}(3-\tau;3) - \mathrm{J01}(3;3-\tau)], \tag{A4g}$$

and

$$4\pi\frac{\partial U^{c}_{33}(\mathbf{x})}{\partial x_3} = m_{\beta}g_{\alpha\beta}s_{\beta}s_{\beta}\gamma_{\alpha}[\mathrm{J01}(1;2) - \mathrm{J01}(2;1)]. \tag{A4h}$$

Functions Cbar( ), I22( ), etc., in equations (A1)–(A4), are those defined exactly in the Ⓔ MATLAB codes in the electronic supplement and are listed below in their exact closed forms in equations (A5)–(A18). The involved parameters and functions in equations (A5)–(A18) are listed in equations (A19)–(A27).

Cbar( ):

$$\bar{C}(\mathbf{x}) = \arctan\frac{\bar{T}^{B}}{V_3} - \arctan\frac{\bar{T}^{A}}{V_3}, \tag{A5}$$

Cbar1( ):

$$\begin{aligned}\bar{\mathrm{C}}^{\xi}_{\sim}(\mathbf{x}) = {}& (-1)^{\xi}\frac{l_3^2}{\bar{L}^4}(l_2^2 - l_1^2)\ln\frac{\bar{R}^{B}}{\bar{R}^{A}} \\ & + (-1)^{\xi}\frac{l_1 l_2 l_3}{\bar{L}^4}(l_1V_1 + l_2V_2 - l_3V_3)\frac{\bar{C}(\mathbf{x})}{V_3} \\ & + (-1)^{\xi}\frac{l_3V_3}{\bar{L}^6}[2l_1l_2W_3 + (l_2^2 - l_1^2)l_3V_3] \\ & \times[(\bar{R}^{B})^{-2} - (\bar{R}^{A})^{-2}] \\ & + (-1)^{\xi}\frac{l_3}{\bar{L}^4}\left(l_1V_2 + l_2V_1 + \frac{4l_1l_2l_3V_3}{\bar{L}^2}\right) \\ & \times[\bar{T}^{B}(\bar{R}^{B})^{-2} - \bar{T}^{A}(\bar{R}^{A})^{-2}],\end{aligned} \tag{A6a}$$

$$\bar{\mathrm{C}}^{\xi}_{ij}(x_1,x_2,x_3) = \bar{\mathrm{C}}^{\xi}_{\sim}(x_1,x_2,x_3^{ij}). \tag{A6b}$$

Remark: Equation (A6b) indicates that to obtain the exact closed-form expression for $\bar{\mathrm{C}}^{\xi}_{ij}(x_1,x_2,x_3)$, one needs only to replace x_3 in $\bar{\mathrm{C}}^{\xi}_{\sim}(x)$ by x_3^{ij}. This is also discussed in the main text.

Cbar2( ):

$$\begin{aligned}\bar{\mathrm{C}}^{\xi\eta}(\mathbf{x}) = {}& -\frac{l_3V_3}{\bar{L}^4}[(-1)^{\xi}l_{3-\xi}l_{\eta} + (-1)^{\eta}l_{\xi}l_{3-\eta}][(\bar{R}^{B})^{-2} - (\bar{R}^{A})^{-2}] \\ & -\frac{l_3}{\bar{L}^4}[(-1)^{\xi+\eta}l_{3-\xi}l_{3-\eta} - l_{\xi}l_{\eta}][\bar{T}^{B}(\bar{R}^{B})^{-2} - \bar{T}^{A}(\bar{R}^{A})^{-2}],\end{aligned} \tag{A7}$$

Cbar3( ):

$$\begin{aligned}\bar{\mathrm{C}}^{\xi\xi\eta}_{\sim}(\mathbf{x}) = {}& \frac{l_3}{2\bar{L}^6}\Big\{4l_{\xi}^2l_{\eta}W_3 + (-1)^{\eta}(2\delta_{\xi\eta}+1)\bar{L}^4V_{3-\eta} + 2[2\varepsilon_{\xi\eta3}\bar{L}^2 \\ & - 3(-1)^{\xi+\eta}(l_2^2 - l_1^2)]l_{3-\eta}l_3V_3\Big\}[(\bar{R}^{B})^{-2} - (\bar{R}^{A})^{-2}] \\ & + (-1)^{\xi}\frac{l_3V_3^2}{\bar{L}^8}\Big[(l_{\eta}^2 - 2l_{3-\eta}^2)l_{\eta}^2V_{3-\eta} + 3l_1l_2l_{3-\eta}^2V_{\eta} \\ & + (4l_{\eta}^2 - l_{3-\eta}^2)l_{3-\eta}l_3V_3\Big][(\bar{R}^{B})^{-4} - (\bar{R}^{A})^{-4}] \\ & - \frac{l_{\eta}l_3^2}{\bar{L}^6}[(2\delta_{\xi\eta}+1)\bar{L}^2 - 4l_{\xi}^2][\bar{T}^{B}(\bar{R}^{B})^{-2} - \bar{T}^{A}(\bar{R}^{A})^{-2}] \\ & + (-1)^{\xi+\eta}\frac{l_3V_3}{\bar{L}^8}\Big[4l_1l_2(l_{\eta}^2V_{3-\eta} + l_{3-\eta}l_3V_3 \\ & + (l_2^2 - l_1^2)^2V_{\eta})\Big][\bar{T}^{B}(\bar{R}^{B})^{-4} - \bar{T}^{A}(\bar{R}^{A})^{-4}],\end{aligned} \tag{A8a}$$

$$\begin{aligned}\bar{\mathrm{C}}^{\xi\xi\eta}_{ij}(x_1,x_2,x_3) &= \bar{\mathrm{C}}^{\xi\xi\eta}_{\sim}(x_1,x_2,x_3^{ij}) \\ \bar{\mathrm{C}}^{\eta\xi\xi}_{ij}(\mathbf{x}) &= \bar{\mathrm{C}}^{\xi\eta\xi}_{ij}(\mathbf{x}) = \bar{\mathrm{C}}^{\xi\xi\eta}_{ij}(\mathbf{x}).\end{aligned} \tag{A8b}$$

Remark: Equation (A8b) is similar to equation (A6b). Namely, to find the expression for the functions with double indexes ij, one just replaces x_3 in the functions by x_3^{ij}.

Cj( ):

$$\mathrm{C}_i(\mathbf{x}) = \frac{L_i^2}{\bar{L}^2}\mathrm{I}^{\sim}_{0;i;3}(\mathbf{x}) - \frac{l_3^2}{\bar{L}^2}s_iB_i(\mathbf{x}) - \frac{l_3W_3}{\bar{L}^2}s_i\frac{A_i(\mathbf{x})}{V_3}. \tag{A9}$$

Remark: Function $\mathrm{I}^{\sim}_{0;i;k}(\mathbf{x})$ and its pair function $\mathrm{I}^{\sim}_{0;ij;k}(\mathbf{x})$ are defined as function I00( ) in equation (A14) below. It is further noted that if we replace x_3 in $\mathrm{C}_i(\mathbf{x})$ by x_3^{ij}, we then obtain its pair function $\mathrm{C}_{ij}(\mathbf{x})$.

Cj2( ):

$$\begin{aligned}\mathrm{C}_i^{\xi\eta}(\mathbf{x}) &= \frac{l_\xi l_\eta}{\bar{L}^4}(2L_i^2-\bar{L}^2)\mathrm{I}^{\sim}_{0;i;3}(\mathbf{x}) - \frac{2s_i l_\xi l_\eta l_3^2}{\bar{L}^4}B_i(\mathbf{x})\\ &\quad - \frac{l_3 V_3}{\bar{L}^2\bar{V}\tilde{V}_i}[l_\xi V_\eta - (-1)^{\xi+\eta} l_{3-\xi}V_{3-\eta}]N_i(\mathbf{x})\\ &\quad - \frac{s_i l_3}{\bar{L}^2}\left[(-1)^\xi l_{3-\xi}V_\eta + (-1)^\eta l_\xi V_{3-\eta} + \frac{2l_\xi l_\eta W_3}{\bar{L}^2}\right]\frac{A_i(\mathbf{x})}{V_3}\\ &\quad - \frac{l_3}{\bar{L}^2\bar{V}}[(-1)^\xi l_{3-\xi}V_\eta + (-1)^\eta l_\xi V_{3-\eta}]P_i(\mathbf{x}).\end{aligned} \tag{A10}$$

Remark: Replacing x_3 in $\mathrm{C}_i^{\xi\eta}(\mathbf{x})$ by x_3^{ij}, we then obtain its pair function $\mathrm{C}_{ij}^{\xi\eta}(\mathbf{x})$.

Cj3( ):

$$\begin{aligned}\mathrm{C}_i^{\xi\xi\eta}(\mathbf{x}) &= \frac{l_\xi^2 l_\eta l_3}{\bar{L}^2 L_i^2}\left(\frac{1}{R_i^B}-\frac{1}{R_i^A}\right)\\ &\quad + \frac{(-1)^\xi l_\xi l_3}{\bar{L}^4 L_i^2\tilde{V}_i^2}\{[(-1)^{\xi+\eta}l_\xi l_{3-\eta} + l_{3-\xi}l_\eta]\bar{L}^2V_3\\ &\quad + (L_i^2+\delta_{\xi\eta}s_i^2 l_3^2)l_{3-\xi}l_\eta V_3\\ &\quad - s_i^2 l_3[(-1)^{\xi+\eta}l_\xi^3 V_{3-\eta} + l_{3-\xi}^2 l_\eta V_{3-\xi}]\}\left(\frac{T_i^B}{R_i^B}-\frac{T_i^A}{R_i^A}\right)\\ &\quad + \frac{l_3 V_{3-\eta}}{\bar{V}^3\tilde{V}_i}\left\{(-1)^\xi\frac{V_3^2}{s_i^2\bar{V}^2}(V_{3-\eta}^2-3V_\eta^2)\right.\\ &\quad \left. + (-1)^\eta[4V_{3-\xi}^2-(2\delta_{\xi\eta}+1)\bar{V}^2]\right\}N_i(\mathbf{x})\\ &\quad - (-1)^\xi\frac{2l_3V_3^2V_{3-\eta}}{\bar{V}^3\tilde{V}_i^3}(V_{3-\eta}^2-3V_\eta^2)\tilde{N}_i(\mathbf{x})\\ &\quad - \frac{(-1)^\xi l_3 V_3^2}{\bar{V}^3\tilde{V}_i}\left\{\frac{V_{3-\eta}}{s_i^2\bar{V}^2}(V_{3-\eta}^2-3V_\eta^2)\right.\\ &\quad \left. - \frac{l_3^2}{\bar{L}^4}[(-1)^\eta V_{3-\eta}(l_2^2-l_1^2)+2l_1l_2V_\eta]\right\}M_i(\mathbf{x})\\ &\quad + (-1)^{\xi+\eta}\frac{l_3V_3V_\eta}{s_i^2\bar{V}^5}(V_\eta^2-3V_{3-\eta}^2)[3P_i(\mathbf{x})\\ &\quad - 2\tilde{P}_i(\mathbf{x})]\\ &\quad - (-1)^{\xi+\eta}\frac{l_3V_3^2}{\bar{V}^3\tilde{V}_i^2}\left\{\frac{l_3}{\bar{L}^4}[l_\eta^3(2V_{3-\eta}^2-V_\eta^2)\right.\\ &\quad + 3l_{3-\eta}(\bar{L}^2V_1V_2 - l_1l_2V_\eta^2)\\ &\quad \left. + \frac{V_3V_\eta}{s_i^2\bar{V}^2}(V_\eta^2-3V_{3-\eta}^2)]\right\}Q_i(\mathbf{x}),\end{aligned} \tag{A11a}$$

$$\mathrm{C}_i^{\eta\xi\xi}(\mathbf{x}) = \mathrm{C}_i^{\xi\eta\xi}(\mathbf{x}) = \mathrm{C}_i^{\xi\xi\eta}(\mathbf{x}), \tag{A11b}$$

CjN( ):

$$\mathrm{C}_i^{-}(\mathbf{x}) = \gamma_i A_i(\mathbf{x}). \tag{A12}$$

Remark: Replacing x_3 in $\mathrm{C}_i^{-}(\mathbf{x})$ by x_3^{ij}, we then obtain its pair function $\mathrm{C}_{ij}^{-}(\mathbf{x})$.

Cjk2( ):

$$\begin{aligned}\mathrm{C}_{i;k}^{\xi\eta}(\mathbf{x}) &= -\frac{l_k l_\xi l_\eta l_3}{\bar{L}^2 L_i^2}\left(\frac{1}{R_i^B}-\frac{1}{R_i^A}\right)\\ &\quad - \frac{l_k}{\bar{L}^4 L_i^2\tilde{V}_i^2}\left\{[(-1)^\xi l_{3-\xi}l_\eta + (-1)^\eta l_\xi l_{3-\eta}]L_i^2 l_3 V_3\right.\\ &\quad - (l_\xi^3 l_\eta + l_\eta^3 l_\xi)W_3 + \delta_{\xi\eta}[l_\xi^4 W_3\\ &\quad \left. - (-1)^\xi l_1 l_2(l_\xi^2 l_3 V_3 + \bar{L}^2 l_\xi V_\xi)]\right\}\left(\frac{T_i^B}{R_i^B}-\frac{T_i^A}{R_i^A}\right)\\ &\quad - \frac{l_k V_3}{s_i^2\bar{V}^3\tilde{V}_i}[(-1)^\xi V_{3-\xi}V_\eta + (-1)^\eta V_\xi V_{3-\eta}]N_i(\mathbf{x})\\ &\quad + \frac{l_k V_3}{\bar{V}\tilde{V}_i}\left\{\frac{1}{s_i^2\bar{V}^2}[(-1)^\xi V_{3-\xi}V_\eta + (-1)^\eta V_\xi V_{3-\eta}]\right.\\ &\quad \left. + \frac{l_3^2}{\bar{L}^4}[(-1)^\xi l_{3-\xi}l_\eta + (-1)^\eta l_\xi l_{3-\eta}]\right\}M_i(\mathbf{x})\\ &\quad + \frac{l_k}{s_i^2\bar{V}^3}[V_\xi V_\eta - (-1)^{\xi+\eta}V_{3-\xi}V_{3-\eta}]P_i(\mathbf{x})\\ &\quad + \frac{l_k V_3}{\bar{V}\tilde{V}_i^2}\left\{-\frac{V_3}{s_i^2\bar{V}^2}[V_\xi V_\eta - (-1)^{\xi+\eta}V_{3-\xi}V_{3-\eta}]\right.\\ &\quad + \frac{l_3}{\bar{L}^4}[(-1)^{\xi+\eta}l_\xi^2(l_\xi V_\eta - 3l_{3-\eta}V_{3-\xi})\\ &\quad \left. - l_{3-\xi}^2(l_{3-\xi}V_{3-\eta} - 3l_\eta V_\xi)]\right\}Q_i(\mathbf{x}),\end{aligned} \tag{A13}$$

I00( ):

$$\mathrm{I}^{\sim}_{0;i;k}(\mathbf{x}) = \frac{l_k}{L_i}\ln\frac{L_i R_i^B - T_i^B}{L_i R_i^A - T_i^A}. \tag{A14}$$

Remark: Replacing x_3 in $\mathrm{I}^{\sim}_{0;i;k}(\mathbf{x})$ by x_3^{ij}, we then obtain its pair function $\mathrm{I}^{\sim}_{0;ij;k}(\mathbf{x})$.

I22( ):

$$\mathrm{I}^{\xi 3}_{2;i;k}(\mathbf{x}) = \frac{l_\xi l_3}{\bar{L}^2}\mathrm{I}^{\sim}_{0;i;k}(\mathbf{x}) - \frac{l_\xi l_k}{\bar{L}^2}\gamma_i B_i(\mathbf{x}) + \frac{(-1)^\xi l_{3-\xi}l_k}{\bar{L}^2}\gamma_i A_i(\mathbf{x}). \tag{A15}$$

Remark: Function $\mathrm{I}^{\sim}_{0;i;k}(\mathbf{x})$ is given in equation (A14); replacing x_3 in $\mathrm{I}^{\xi 3}_{2;i;k}(\mathbf{x})$ by x_3^{ij}, we then obtain its pair function $\mathrm{I}^{\xi 3}_{2;ij;k}(\mathbf{x})$.

J01( ): Listed below are J01$(\xi;k)$ and J01$(3;k)$,

$$\begin{aligned}\mathrm{J}^{\xi}_{0;i;k}(\mathbf{x}) &= -\frac{l_\xi l_k}{L_i^2}\left(\frac{1}{R_i^B}-\frac{1}{R_i^A}\right)\\ &\quad+\frac{l_k}{L_i^2\tilde{V}_i^2}[(-1)^{\xi}(s_i^2 l_3 V_{3-\xi}-l_{3-\xi}V_3)]\left(\frac{T_i^B}{R_i^B}-\frac{T_i^A}{R_i^A}\right)\\ \mathrm{J}^{3}_{0;i;k}(\mathbf{x}) &= -\frac{l_3 l_k}{L_i^2}\left(\frac{1}{R_i^B}-\frac{1}{R_i^A}\right)+\frac{l_k}{L_i^2\tilde{V}_i^2}W_3\left(\frac{T_i^B}{R_i^B}-\frac{T_i^A}{R_i^A}\right).\end{aligned} \tag{A16}$$

Remark: Replacing x_3 in $\mathrm{J}^{m}_{0;i;k}(\mathbf{x})$ by x_3^{ij} $(m=1,2,3)$, we then obtain its pair function $\mathrm{J}^{m}_{0;ij;k}(\mathbf{x})$.

L21( ):

$$\mathrm{L}^{\xi}_{2;\sim k}(\mathbf{x}) = \frac{l_\xi l_k}{\bar{L}^2}\ln\frac{\bar{R}^B}{\bar{R}^A}-\frac{(-1)^{\xi}l_{3-\xi}l_k}{\bar{L}^2}\bar{C}(\mathbf{x}), \tag{A17}$$

L43( ):

$$\begin{aligned}\mathrm{L}^{123}_{4;\sim;3}(\mathbf{x}) &= \frac{l_1 l_2 l_3^2}{\bar{L}^4}\ln\frac{\bar{R}^B}{\bar{R}^A}+\frac{l_3^2}{2\bar{L}^4}(l_2^2-l_1^2)\bar{C}(\mathbf{x})\\ &\quad+\frac{l_3 V_3}{2\bar{L}^6}(l_1^3V_2+l_2^3V_1+3l_1l_2l_3V_3)[(\bar{R}^B)^{-2}-(\bar{R}^A)^{-2}]\\ &\quad-\frac{l_3}{2\bar{L}^6}[2l_1l_2W_3+l_3V_3(l_2^2-l_1^2)][\bar{T}^B(\bar{R}^B)^{-2}-\bar{T}^A(\bar{R}^A)^{-2}],\end{aligned} \tag{A18a}$$

$$\mathrm{L}^{123}_{4;ij;3}(x_1,x_2,x_3) = \mathrm{L}^{123}_{4;\sim 3}(x_1,x_2,x_3^{ij}). \tag{A18b}$$

Remark: It is noted that the superscripts 123 in this L-function correspond to the subscripts in l and V.

In equations (A1)–(A18), the involved functions and parameters are defined as

$$\begin{aligned}A_i(\mathbf{x}) &= \arctan\frac{s_i\bar{V}M_3^B}{V_3\sqrt{(\tilde{V}_i d_3^B)^2+(M_3^B)^2}}\\ &\quad-\arctan\frac{s_i\bar{V}M_3^A}{V_3\sqrt{(\tilde{V}_i d_3^A)^2+(M_3^A)^2}},\end{aligned} \tag{A19}$$

$$\begin{aligned}B_i(\mathbf{x}) &= \ln\frac{\sqrt{(\tilde{V}_i d_3^B)^2+(M_3^B)^2}-s_i\bar{V}d_3^B}{\sqrt{(V_3 d_3^B)^2+(M_3^B)^2}}\\ &\quad-\ln\frac{\sqrt{(\tilde{V}_i d_3^A)^2+(M_3^A)^2}-s_i\bar{V}d_3^A}{\sqrt{(V_3 d_3^A)^2+(M_3^A)^2}}\\ &= \ln\frac{\sqrt{(V_3 d_3^B)^2+(M_3^B)^2}}{\sqrt{(\tilde{V}_i d_3^B)^2+(M_3^B)^2}+s_i\bar{V}d_3^B}\\ &\quad-\ln\frac{\sqrt{(V_3 d_3^A)^2+(M_3^A)^2}}{\sqrt{(\tilde{V}_i d_3^A)^2+(M_3^A)^2}+s_i\bar{V}d_3^A},\end{aligned} \tag{A20}$$

$$M_i(\mathbf{x}) = \frac{\tilde{V}_i d_3^B}{\sqrt{(\tilde{V}_i d_3^B)^2+(M_3^B)^2}}-\frac{\tilde{V}_i d_3^A}{\sqrt{(\tilde{V}_i d_3^A)^2+(M_3^A)^2}}, \tag{A21}$$

$$\begin{aligned}N_i(\mathbf{x}) &= \frac{(\tilde{V}_i d_3^B)\sqrt{(\tilde{V}_i d_3^B)^2+(M_3^B)^2}}{(V_3 d_3^B)^2+(M_3^B)^2}\\ &\quad-\frac{(\tilde{V}_i d_3^A)\sqrt{(\tilde{V}_i d_3^A)^2+(M_3^A)^2}}{(V_3 d_3^A)^2+(M_3^A)^2},\end{aligned} \tag{A22}$$

$$\begin{aligned}\tilde{N}_i(\mathbf{x}) &= \frac{(\tilde{V}_i d_3^B)^3\sqrt{(\tilde{V}_i d_3^B)^2+(M_3^B)^2}}{[(V_3 d_3^B)^2+(M_3^B)^2]^2}\\ &\quad-\frac{(\tilde{V}_i d_3^A)^3\sqrt{(\tilde{V}_i d_3^A)^2+(M_3^A)^2}}{[(V_3 d_3^A)^2+(M_3^A)^2]^2},\end{aligned} \tag{A23}$$

$$P_i(\mathbf{x}) = \frac{M_3^B\sqrt{(\tilde{V}_i d_3^B)^2+(M_3^B)^2}}{(V_3 d_3^B)^2+(M_3^B)^2}-\frac{M_3^A\sqrt{(\tilde{V}_i d_3^A)^2+(M_3^A)^2}}{(V_3 d_3^A)^2+(M_3^A)^2}, \tag{A24}$$

$$\begin{aligned}\tilde{P}_i(\mathbf{x}) &= \frac{M_3^B[\sqrt{(\tilde{V}_i d_3^B)^2+(M_3^B)^2}]^3}{[(V_3 d_3^B)^2+(M_3^B)^2]^2}\\ &\quad-\frac{M_3^A[\sqrt{(\tilde{V}_i d_3^A)^2+(M_3^A)^2}]^3}{[(V_3 d_3^A)^2+(M_3^A)^2]^2},\end{aligned} \tag{A25}$$

$$Q_i(\mathbf{x}) = \frac{M_3^B}{\sqrt{(\tilde{V}_i d_3^B)^2 + (M_3^B)^2}} - \frac{M_3^A}{\sqrt{(\tilde{V}_i d_3^A)^2 + (M_3^A)^2}}, \tag{A26}$$

in which

$$\begin{aligned}
&\mathbf{x}^A = (x_1^A, x_2^A, x_3^A),\ \mathbf{x}^B = (x_1^B, x_2^B, x_3^B),\ \mathbf{x} = (x_1, x_2, x_3),\\
&\mathbf{d}^A = \mathbf{x} - \mathbf{x}^A = (d_1^A, d_2^A, d_3^A),\ \mathbf{d}^B = \mathbf{x} - \mathbf{x}^B = (d_1^B, d_2^B, d_3^B),\\
&\mathbf{l} = \mathbf{x}^B - \mathbf{x}^A = (l_1, l_2, l_3),\\
&\bar{L} = \sqrt{l_1^2 + l_2^2},\quad L_i = \sqrt{\bar{L}^2 + s_i^2 l_3^2},\\
&\mathbf{M}^A = \mathbf{d}^A \times (\mathbf{d}^A \times \mathbf{l}) = (M_1^A, M_2^A, M_3^A),\\
&\mathbf{M}^B = \mathbf{d}^B \times (\mathbf{d}^B \times \mathbf{l}) = (M_1^B, M_2^B, M_3^B),\\
&\bar{R}^A = \sqrt{(d_1^A)^2 + (d_2^A)^2},\quad \bar{R}^B = \sqrt{(d_1^B)^2 + (d_2^B)^2},\\
&R_i^A = \sqrt{(d_1^A)^2 + (d_2^A)^2 + s_i^2 (d_3^A)^2},\\
&R_i^B = \sqrt{(d_1^B)^2 + (d_2^B)^2 + s_i^2 (d_3^B)^2},\\
&\bar{T}^A = l_1 d_1^A + l_2 d_2^A,\quad \bar{T}^B = l_1 d_1^B + l_2 d_2^B,\\
&T_i^A = \bar{T}^A + s_i^2 l_3 d_3^A,\quad T_i^B = \bar{T}^B + s_i^2 l_3 d_3^B,\\
&\mathbf{V} = \mathbf{d}^A \times \mathbf{l} = \mathbf{d}^B \times \mathbf{l} = (V_1, V_2, V_3),\\
&\bar{V} = \sqrt{V_1^2 + V_2^2},\quad \tilde{V}_i = \sqrt{s_i^2 \bar{V}^2 + V_3^2},\\
&\mathbf{W} = \mathbf{l} \times (\mathbf{d}^A \times \mathbf{l}) = \mathbf{l} \times (\mathbf{d}^B \times \mathbf{l}) = (W_1, W_2, W_3).
\end{aligned} \tag{A27}$$

Appendix B

Detailed Function Relations Between Those Defined in this Article and Those in the Supplemental MATLAB Codes

Cbar( ) ≡ Cbar(TbarA,TbarB,V);

Cbar1( ) ≡ Cbar1(ks,l,d33A,d33B,V33,W33,Lbar,Rbar33A,Rbar33B,Tbar33A,Tbar33B);

Cbar2( ) ≡ Cbar2(it,ks,l,d33A,d33B,V33,Lbar,Rbar33A,Rbar33B,Tbar33A,Tbar33B);

Cbar3( ) ≡ Cbar3(it,ks,t,l,d33A,d33B,V33,W33,Lbar,Rbar33A,Rbar33B,Tbar33A,Tbar33B);

Cj( ) ≡ Cj(gamaj,l,dA,dB,V,W,MA,MB,Vbar,Vj,Lbar,Lj,RjA,RjB,TjA,TjB);

Cj2( ) ≡ Cj2(1,2,gamaj,l,dA,dB,V,W,MA,MB,Vbar,Vj,Lbar,Lj,RjA,RjB,TjA,TjB);

Cj3( ) ≡ Cj3(it,ks,t,gamaj,l,dA,dB,V,MA,MB,Vbar,Vj,Lbar,Lj,RjA,RjB,TjA,TjB);

CjN( ) ≡ CjN(gama3,dA,dB,V,MA,MB,Vbar,V3);

Cjk2( ) ≡ Cjk2(it,t,gamaj,ks,l,dA,dB,V,W,MA,MB,Vbar,Vj,Lbar,Lj,RjA,RjB,TjA,TjB);

I00( ) ≡ I00(3,l,L3,R3A,R3B,T3A,T3B);

I22( ) ≡ I22(ks,gamaj,3-ks,l,dA,dB,V,MA,MB,Vbar,Vj,Lbar,Lj,RjA,RjB,TjA,TjB);

J01(3-t;l) ≡ J01(3,gama3,3-t,l,V,W,V3,L3,R3A,R3B,T3A,T3B);

L21( ) ≡ L21(ks,l,d33A,d33B,V33,Lbar,Rbar33A,Rbar33B,Tbar33A,Tbar33B);

L43( ) ≡ L43(l,d33A,d33B,V33,W33,Lbar,Rbar33A,Rbar33B,Tbar33A,Tbar33B).

Department of Civil Engineering
University of Akron
Akron, Ohio 44325
pan2@uakron.edu
(E.P.)

AML, Department of Engineering Mechanics
Tsinghua University
Beijing 100084, China
yuanjianghong1984@gmail.com
(J.H.Y.)

Department of Engineering Mechanics
Zhejiang University
Hangzhou 310027, China
chenwq@zju.edu.cn
(W.Q.C.)

Department of Earth and Environmental Sciences
University of Texas at Arlington
Arlington, Texas 76019
wagriff@uta.edu
(W.A.G.)

Manuscript received 7 June 2014;
Published Online 11 November 2014